

1

2 **Global drought and severe drought affected population in 1.5°C**
3 **and 2°C warmer worlds**

4

5 Wenbin Liu^a, Fubao Sun^{a,b,c,d*}, Wee Ho Lim^{a,e}, Jie Zhang^a, Hong Wang^a,

6 Hideo Shiogama^f and Yuqing Zhang^g

7

8 ^a Key Laboratory of Water Cycle and Related Land Surface Processes, Institute of Geographic
9 Sciences and Natural Resources Research, Chinese Academy of Sciences, Beijing, China

10 ^b Ecology Institute of Qilian Mountain, Hexi University, Zhangye, China

11 ^c College of Resources and Environment, University of Chinese Academy of Sciences, Beijing,
12 China

13 ^d Center for Water Resources Research, Chinese Academy of Sciences, Beijing, China

14 ^e Environmental Change Institute, University of Oxford, Oxford, UK

15 ^f Center for Global Environmental Research, National Institute for Environmental Studies, Tsukuba,
16 Japan

17 ^g College of Atmospheric Sciences, Nanjing University of Information Science and Technology,
18 Nanjing, China

19

20 **Pre-submit to:** Earth System Dynamics (*Special issue: Earth System at a 1.5°C warming world*)

21 **Corresponding to:** Prof. Fubao Sun (sunfb@igsnrr.ac.cn), Institute of Geographic Sciences and
22 Natural Resources Research, Chinese Academy of Sciences

23

24 2018/3/5

25

26 **Abstract.** The 2015 Paris Agreement proposed a more ambitious climate change mitigation target,
27 on limiting the global warming at 1.5°C instead of 2°C above pre-industrial levels. Scientific
28 investigations on environmental risks associated with these warming targets are necessary to
29 inform climate policymaking. Based on the CMIP5 (the fifth Coupled Model Intercomparison
30 Project) climate models, we present the first risk-based assessment of changes in global drought
31 and the impact of severe drought on population at 1.5°C and 2°C additional warming conditions.
32 Our results highlight the risk of drought at the globe (drought duration would increase from 2.9
33 to 3.1~3.2 months) and in several hotspot regions such as Amazon, Northeastern Brazil, South
34 Africa and Central Europe at both 1.5 °C and 2 °C global warming relative to the historical period.
35 Correspondingly, more total and urban population would be exposed to severe droughts at the
36 globe (+132.5±216.2 million and +194.5±276.5 million total population, +350.2±158.8 million and
37 +410.7±213.5 million urban population in 1.5 °C and 2 °C warmer worlds) and some regions (i.e.,
38 East Africa, West Africa and South Asia). Less rural population (-217.7±79.2 million and
39 -216.2±82.4 million rural population in 1.5 °C and 2 °C warmer worlds) would be exposed to
40 severe drought at the globe under both climate warming and population growth (especially the
41 urbanization-induced population migration). By keeping global warming at 1.5°C above the
42 pre-industrial levels instead of 2°C, drought risks would decrease (i.e., less drought duration,
43 drought intensity and drought severity but relatively more frequent severe drought) and the
44 affected total, urban and rural population would decrease at the globe and in most regions.
45 Whilst challenging for both East Africa and South Asia, the benefits of limiting warming to below
46 1.5°C in terms of global drought risk and impact reduction are significant.

47

48 **1 Introduction**

49 Drought could bring adverse consequences on water supplies, food productions and the
50 environment (Wang et al., 2011; Sheffield et al., 2012). Because of these serious consequences,
51 severe droughts in the recent past have gained wide attentions, these include the Millennium
52 drought in Southeast Australia (van Dijk et al., 2013; Kiem et al., 2016), the once-in-a-century
53 droughts in Southwest China (Qiu, 2010, Zuo et al., 2015), the Horn of Africa drought (Masih et
54 al., 2014; Lyon, 2014) and the most recent California drought (Aghakouchak et al., 2015; Cheng et
55 al., 2016). In the context of climate change, drought risks (i.e., drought duration and intensity) are
56 likely to increase in many historical drought-prone regions with global warming (Dai et al., 2012;
57 Fu and Feng, 2014; Kelley et al., 2015; Ault et al., 2016). A better understanding of changes in
58 global drought characteristics and their socioeconomic impacts in the 21st century should feed
59 into long-term climate adaptation and mitigation plans.

60

61 The United Nations Framework Convention on Climate Change (UNFCCC) agreed to establish a
62 long-term temperature goal for climate projection of “*pursue efforts to limit the temperature*
63 *increase to 1.5°C above pre-industrial levels, recognizing that this would significantly reduce the*
64 *risks and impacts of climate change*” (UNFCCC Conference of the Parties, 2015) in the 2015 Paris
65 Agreement, and invited the Intergovernmental Panel on Climate Change (IPCC) to announce a
66 special report “*On the impacts of global warming of 1.5°C above pre-industrial levels and related*
67 *greenhouse gas emission pathways*” in 2018 (Mitchell et al., 2016). Regardless of the
68 socio-economic and political achievability of this goals (Sanderson et al., 2017), there is a paucity
69 of scientific knowledge about the relative risks (i.e., drought risks and their potential impacts)

70 associated with the implications of 1.5°C and/or 2°C warming, this naturally attracted
71 contributions from scientific community (Hulme 2016, Schleussner et al., 2016, Peters 2016, King
72 et al., 2017).

73

74 To target on the impact assessments of 1.5°C and/or 2°C warming, there are currently several
75 approaches (James et al., 2017). One way is to enable impact assessments at near-equilibrium
76 climate of 1.5°C and/or 2°C warmer worlds designed specifically using a set of ensemble
77 simulations produced by a coupled climate model (i.e., Community Earth System Model, CESM)
78 (Sanderson et al., 2017; Wang et al., 2017). Although similar results of drought response to
79 warming were obtained as that conducted by Coupled Model Intercomparison Project-style
80 experiments (i.e., CMIP5, Taylor et al., 2012), the structural uncertainty and robustness of change
81 in droughts among different climate models cannot be fully evaluated in this kind of single-model
82 study (Lehner et al., 2017). A second approach extends the former idea to multiple climate
83 models. For instance, the HAPPI (Half a degree Additional warming, Projections, Prognosis and
84 Impacts) model intercomparison project provided a new assessment framework and a dataset
85 with experiment design target explicitly to 1.5°C and 2°C above the pre-industrial levels (Mitchell
86 et al., 2017). However, the analysis/calculation of drought characteristics needs data with
87 long-term period (typically >20 consecutive years, McKee et al., 1993), the ten-year period HAPPI
88 dataset (i.e., 2005-2016 for the historical period and 2105-2116 for the 1.5°C and 2°C warmer
89 worlds) is relatively short (consecutive samples are too short for calculating a drought index, i.e.,
90 Palmer drought severity index (PDSI), Palmer, 1965) for an index-based drought assessment. A
91 third approach utilizes the outputs of CMIP5 climate models under the RCP2.6 scenarios for this

92 kind of “risk assessment-style” studies, but only a handful of General Circulation Models (GCMs)
93 simulations end up showing 1.5°C global warming by end of the 21st century. Alternatively,
94 transient simulations from multiple CMIP5 GCMs at higher greenhouse emissions (i.e., RCP4.5
95 and RCP8.5) (Schleussner et al., 2016; King et al., 2017) could be analyzed in order to evaluate the
96 potential risks of drought under different warming targets, albeit the long-duration drought years
97 might be underestimated due to insufficient sampling of extended drought events (Lehner et al.,
98 2017).

99

100 Here, we quantify the changes in global and sub-continental drought characteristics (i.e., drought
101 duration, intensity and severity) at 1.5°C and 2°C above the pre-industrial levels and find out
102 whether there are significant differences between them. We perform this analysis using a
103 drought index-PDSI forced by the latest CMIP5 GCMs. To evaluate the societal impacts, we
104 incorporate the Shared Socioeconomic Pathway 1 (SSP1) spatial explicit global population
105 scenario and examine the exposure of population (including rural, urban and total population) to
106 severe droughts. This paper is organized as follows: Section 2 introduces the CMIP5 GCMs output
107 and SSP1 population data applied in this study. We define the baseline, 1.5°C and 2°C warmer
108 world; and describe the calculation of PDSI-based drought characteristics and population
109 exposure under severe droughts in this section. Section 3 shows the results (i.e., hotspots and
110 risks) of changes in drought characteristics and the impacts of severe drought on people under
111 these warming targets. We perform detailed discussions in Section 4 and conclude our findings in
112 Section 5.

113

114 **2 Material and Methods**

115 **2.1 Data**

116 In this study, we use the CMIP5 GCMs output (including the monthly outputs of surface mean air
117 temperature, surface minimum air temperature, surface maximum air temperature, air pressure,
118 precipitation, relative humidity, surface downwelling longwave flux, surface downwelling
119 shortwave flux, surface upwelling longwave flux and surface upwelling shortwave flux as well as
120 the daily outputs of surface zonal velocity component (*uwnd*) and meridional velocity
121 component (*vwnd*)) archived at the Earth System Grid Federation (ESGF) Node at the German
122 Climate Computing Center-DKRZ (<https://esgf-data.dkrz.de/projects/esgf-dkrz/>) over the period
123 1850-2100. In the CMIP5 archive, the monthly *uwnd* and *vwnd* were computed as the means
124 of their daily values with the plus-minus sign, the calculated wind speed from the monthly *uwnd*
125 and *vwnd* would be equal to or, in most cases, less than that computed from the daily values
126 (Liu and Sun, 2016, 2017). To get the monthly wind speed, we average the daily values
127 $(\sqrt{uwnd^2 + vwnd^2})$ over a month.

128

129 Recent studies have confirmed that the impacts of similar global mean surface temperature (i.e.,
130 1.5°C and 2°C warmer worlds) among the Representative Concentration Pathways (RCPs) are
131 quite similar, implying that the global and regional responses to temperature and are
132 independent of the RCPs (Hu et al., 2017; King et al., 2017). Following this idea, we settled at
133 using 11 CMIP5 models which satisfied the data requirement of PDSI calculation (see paragraph
134 above) under RCP4.5 and RCP8.5. Following Wang et al. (2017) and King et al. (2017), we use the

135 ensemble mean of these CMIP5 models and climate scenarios (RCP4.5, RCP8.5) to composite the
136 warming scenarios (1.5°C and 2°C warmer worlds).

137 <Table 1, here, thanks>

138 To consider the people affected by severe drought events, we use the spatial explicit global
139 population scenarios developed by researchers from the Integrated Assessment Modeling (IAM)
140 group of National Center for Atmospheric Research (NCAR) and the City University of New York
141 Institute for Demographic Research (Jones and O’Neil, 2016). They included the gridded
142 population data for the baseline year (2000) and for the period of 2010-2100 in ten-year steps at
143 a spatial resolution of 0.125 degree, which are consistent with the new Shared Socioeconomic
144 Pathways (SSPs). We apply the population data of the SSP1 scenario, which describes a future
145 pathway with sustainable development and low challenges for adaptation and mitigation. We
146 upscale this product to a spatial resolution of 0.5° × 0.5°. For the global and sub-continental scales
147 analysis, we use the global land mass between 66°N and 66°S (Fischer et al., 2013; Schleussner et
148 al., 2016) and 26 sub-continental regions (as used in IPCC, 2012, see Table 2 for details).

149 <Table 2, here, thanks>

150 **2.2 Definition of a baseline, 1.5°C and 2°C warmer worlds**

151 To define a baseline, 1.5°C and 2°C warmer worlds, we first calculate the global mean surface air
152 temperature (GMT) for each climate model and emission scenario over the period 1850-2100.

153 We weigh the surface air temperature field by the square root of cosine (latitude) to consider the
154 dependence of grid density on latitude (Liu et al., 2016). We compute and smooth the
155 multi-model Ensemble Mean (MEM) GMT using a 20-year moving average filter for the RCP4.5
156 and RCP8.5, respectively. This study applied continuous time series for identification of drought

157 duration, intensity and severity. From the climate model projections, we noticed that
158 inter-annual variation of global mean air temperature is common and its magnitude differs with
159 different climate models. To account for it, following Wang et al. (2017), we first select a baseline
160 period of 1986-2005 for which the observed GMT was about 0.6°C warmer (the MEM GMT was
161 0.4~0.8 °C warmer during this period in 11 climate models used) than the pre-industrial levels
162 (1850-1900, IPCC, 2013). This is also a common reference period for climate impact assessment
163 (e.g., Schleussner et al., 2016). Next, for each emission scenario (RCP4.5 or RCP8.5), we define
164 the periods (Figure 1) during which the 20-year smoothed GMT increase by 1.3~1.7 °C
165 (2027-2038 under the RCP4.5 and 2029-2047 under the RCP 8.5) and by 1.8~2.2 °C (2053-2081
166 under the RCP4.5 and 2042-2053 under the RCP 8.5) above the pre-industrial period as the 1.5°C
167 and 2°C warmer worlds, respectively (as in King et al., 2017). To reduce the projection uncertainty
168 inherited from different emission scenarios, we combine (by averaging) the results of drought
169 characteristics and population exposures calculated for selected periods under the RCP4.5 and
170 RCP8.5, to represent the ensemble means of drought risk at 1.5°C or 2°C warmer worlds. In the
171 1.5°C and 2°C warmer worlds, we get 372 and 492 monthly data-points, respectively.

172 <Figure 1, here, thanks>

173 **2.3 Characterize global drought using PDSI**

174 To quantify the changes in drought characteristics, we adopt the Palmer Drought Severity index
175 (PDSI), which describes the balance between water supply (precipitation) and atmospheric
176 evaporative demand (required “precipitation” estimated under climatically appropriate for
177 existing conditions, CAFEC) at the monthly scale (Wells et al., 2004; Zhang et al., 2016). For a
178 multiyear time series, this index is commonly applied as an indication of a meteorological

179 drought; to a lesser extent, a hydrological drought (Heim Jr., 2002; Zargar et al., 2011; Hao et al.,
 180 2018). It incorporates antecedent precipitation, potential evaporation and the local Available
 181 Water Content (AWC, links: https://daac.ornl.gov/cgi-bin/dsviewer.pl?ds_id=548) of the soil in
 182 the hydrological accounting system. It measures the cumulative departure relative to the local
 183 mean conditions in atmospheric moisture supply and demand on land surface. In the PDSI model,
 184 five surface water fluxes, namely, precipitation (P), recharge to soil (R), actual evapotranspiration
 185 (E), runoff (RO) and water loss to the soil layers (L); and their potential values \hat{P} , PR , PE , PRO and
 186 PL are considered. All values in the model can be computed under CAFEC values using the
 187 precipitation, potential evaporation and AWC inputs. For example, the CAFEC precipitation (\hat{P}) is
 188 defined as (Dai et al., 2011),

$$189 \quad \hat{P} = \frac{\bar{E}_t}{\bar{PE}_t} PE + \frac{\bar{R}_t}{\bar{PR}_t} PR + \frac{\bar{RO}_t}{\bar{PRO}_t} PRO - \frac{\bar{L}_t}{\bar{PL}_t} PL, \quad (1)$$

190 In Equation 1, the over bar indicates averaging of a parameter over the calibration period. The
 191 moisture anomaly index (Z index) is derived as the product of the monthly moisture departure
 192 ($P - \hat{P}$) and a climate characteristics coefficient K . The Z index is then applied to calculate the
 193 PDSI value for time $t(X_t)$:

$$194 \quad X_t = pX_{t-1} + qZ_t = 0.897X_{t-1} + Z_t/3 \quad (2)$$

195 Where X_{t-1} is the PDSI of the previous month, and p and q are duration factors. The
 196 calculated PDSI ranges -10 (dry) to 10 (wet). The parameters (i.e., the duration factor) in PDSI
 197 model are calibrated using the period 1850-2000 (see Section 2.2).

198

199 As part of the PDSI calculation, we quantify the potential evaporation (PET) using the Food and
 200 Agricultural Organization (FAO) Penman-Monteith equation (Allen et al., 1998),

201
$$PET = \frac{0.408\Delta(R_n - G) + \gamma \frac{900}{T + 273} U_2 e_s \left(1 - \frac{Rh}{100}\right)}{\Delta + \gamma(1 + 0.34U_2)} \quad (3)$$

202 where Δ is the slope of the vapor pressure curve, U_2 is the wind speed at 2 m height, G is the
 203 soil heat flux, Rh is the relative humidity, γ is the psychrometric constant, e_s is the saturation
 204 vapor pressure at a given air temperature (T). R_n is the net radiation which can be calculated
 205 using the surface downwelling/upwelling shortwave and longwave radiations. We estimate all
 206 other parameters in the FAO Penman-Monteith equation using the GCM outputs through the
 207 standard algorithm as per recommended by the FAO (Allen et al., 1998). In this study, we perform
 208 this calculation for each GCM over the period 1850-2100 using the tool for calculating the PDSI
 209 (the original MATLAB codes were modified for this case) developed by Jacobi et al. (2013).

210

211 Based on the calculated global PDSI, we derive the drought characteristics (i.e., drought duration,
 212 drought intensity and drought severity) using the run theory for the baseline, 1.5°C and 2°C
 213 warmer worlds, respectively. Briefly, the concept of “run theory” is proposed by Yevjevich and
 214 Ingenieur (1967). The run characterizes the statistical properties of sequences in both time and
 215 space. It is useful for defining drought in an objective manner. In the run theory, a “run”
 216 represents a portion of time series X_i , where all values are either below or above a specified
 217 threshold (we set the threshold PDSI < -1 in this study) (Ayantobo et al., 2017). We define a “run”
 218 with values continuously stay below that threshold (i.e., negative run) as a drought event, which
 219 generally includes these characteristics: drought duration, drought intensity and drought severity
 220 (see Figure 2 for better illustration). We define the drought duration (months in this study) as a
 221 period (years/months/weeks) which PDSI stays below a specific threshold (PDSI < -1). Drought
 222 severity (dimensionless) indicates a cumulative deficiency of a drought event below the threshold

223 (PDSI < -1), while drought intensity (dimensionless) is the average value of a drought event below
224 this threshold (Mishra and Singh, 2010). For each GCM, we calculate the medians of drought
225 duration, drought intensity and drought severity at each grid-cell across all drought events for
226 each selected period (i.e., the baseline, 1.5°C and 2°C warmer worlds). It should be noted that
227 the global PDSI and related drought characteristics were first calculated using GCM-outputs with
228 their original spatial resolution. The obtained results were then rescaled to a common spatial
229 resolution of 0.5° × 0.5° using the bilinear interpolation, in order to show them with a finer
230 resolution uniformly and accommodate their spatial resolution to that of SSP1 population (0.5°
231 × 0.5°). The original resolution of SSP1 population is 0.125 degree. We thus use a 0.5 degree
232 resolution to avoid effectively making up data of the finer resolution in SSP1 data. We synthesize
233 the results by evaluating the ensemble mean and model consistency/inter-model variance across
234 all climate models.

235 <Figure 2, here, thanks>

236 **2.4 Calculation of population exposure under severe droughts**

237 Following Wells et al. (2014), when monthly PDSI < -3, we assume a severe drought event took
238 place. If a severe drought occurred for at least a month in a year, we would take that year as a
239 severe drought year. For each GCM per period (i.e., the baseline, 1.5°C and 2°C warmer worlds),
240 we quantify the population (including urban, rural and all population) affected by severe drought
241 per grid-cell as (population × annual frequency of severe drought). We first compute the
242 affected population for the baseline period (1985-2005) using the SSP1 base year (2000). We
243 repeat this estimation using the constant SSP1 population data in 2100 for the 1.5°C and 2°C
244 warmer worlds, which is consistent with the original proposal of Paris Agreement on stabilizing

245 global warming for the specified targets by end of the 21st century. We used SSP1 scenario
246 because it describes the storyline of a green growth paradigm with sustainable development and
247 low challenges for adaptation and mitigation (Jones and O’Niell, 2016). The 1.5°C and 2°C
248 warmer worlds clearly fit in this description and thus considered under the 2015 Paris Agreement
249 (UNFCCC Conference of the Parties 2015; O’Niell et al., 2016). In this pathway, the world
250 population would peak at around 2050s and then decline (van Vuuren et al., 2017). The
251 environmental friendly living arrangements and human settlement design in this scenario would
252 lead to fast urbanization in all countries. More in-migrants from rural areas would be attracted to
253 cities due to more adequate infrastructure, employment opportunities and convenient services
254 for their residents (Cuaresma, 2012). The world urban population would gradually increase while
255 rural population would correspondingly decline in the future under SSP1 scenario.

256

257 **3 Results**

258 **3.1 Changes in PDSI and drought characteristics**

259 We present the changes in multi-model ensemble mean PDSI from the baseline period
260 (1986-2005) to each of the 1.5°C and 2°C warmer worlds and model consistency in Figure 3. For
261 the 1.5°C warmer world, the PDSI would decrease (more drought-prone) with relatively high
262 model consistency (6~11 models in totally 11 climate models) in some regions, for example,
263 Amazon ($0.7 \pm 0.8 \rightarrow -0.1 \pm 0.2$), Northeastern Brazil ($0.5 \pm 0.6 \rightarrow -0.1 \pm 0.3$), Southern Europe and
264 Mediterranean ($0.4 \pm 0.6 \rightarrow -0.3 \pm 0.2$), Central America and Mexico ($0.2 \pm 0.4 \rightarrow -0.2 \pm 0.1$), Central
265 Europe ($0.3 \pm 1.0 \rightarrow -0.1 \pm 0.4$) as well as Southern Africa ($0.5 \pm 0.5 \rightarrow -0.3 \pm 0.2$); slightly increase (less
266 drought-prone) in Alaska/Northwest Canada ($-0.01 \pm 0.5 \rightarrow -0.3 \pm 0.2$) and North Asia ($-0.1 \pm 1.0 \rightarrow$

267 -0.2±0.2) but with relatively low model consistency. The geographic pattern of changes in PDSI for
268 the 2°C warmer world is quite similar to that of 1.5°C warmer world, but the magnitude of
269 change would intensify (both directions) in East Canada, Greenland, Iceland (-0.3±0.2-> -0.4±0.2),
270 East Africa (-0.5±0.2-> -0.3±0.2), Northern Europe (-0.3±0.3-> -0.2±0.3), East Asia (-0.3±0.1->
271 -0.2±0.4), South Asia (-1.0±1.2-> -0.8±0.3) and West Africa (-0.3±0.2-> -0.3±0.3). When global
272 warming is capped at 1.5°C instead of 2°C above the pre-industrial levels, the PDSI value would
273 elevate at the globe (66°S-66°S, -0.4±0.2-> -0.3±0.2) and most regions (Alaska/Northwest Canada,
274 East Africa, West Africa, Tibetan Plateau, North Asia, East Asia, South Asia and Southeast Asia)
275 (Figure 4).

276 <Figure 3, here, thanks>

277 <Figure 4, here, thanks>

278 We analyze the changes in drought characteristics such as its duration, severity and intensity in
279 1.5°C and 2°C warmer worlds. In terms of the drought duration (Figures 5-6), we find robust
280 large-scale features. For example, the drought duration would generally increase at the globe
281 (2.9±0.5 -> 3.1±0.4 months and 2.9±0.5 -> 3.2±0.5 months from the baseline period to the 1.5°C
282 and 2°C warmer worlds) and most regions (especially for Amazon, Sahara, Northeastern Brazil
283 and North Australia) except for North Asia (2.7±0.6 -> 2.6±0.5 months and 2.7±0.6 -> 2.5±0.4
284 months) in both worlds. The high model consistency in most regions (i.e., Amazon, Sahara and
285 Northeastern Brazil) for both warming targets gives us more confidence on these projections.
286 Relative to the 2°C warming target, a 1.5°C warming target is more likely to reduce drought
287 duration at both global and regional scales (except for Alaska/Northwest Canada, East Africa,
288 Sahara, North Europe, North Asia, South Asia, Southeast Asia, Tibetan Plateau and West Africa).

289 <Figure 5, here, thanks>

290 <Figure 6, here, thanks>

291 Drought intensity and drought severity are commonly used for quantifying the extent of water
292 availability drops significantly below normal conditions in a region. In this study, the drought
293 intensity is projected to increase at the globe ($0.9\pm0.3 \rightarrow 1.1\pm0.3$ and $0.9\pm0.3 \rightarrow 1.0\pm0.2$ from the
294 baseline period to the 1.5°C and 2°C warmer worlds) and in most of the regions except for North
295 Asia, Southeast Asia and West Africa in 1.5°C and 2°C warmer worlds (Figures 7-8). Compare to
296 the 2°C warmer world, the drought intensity would obviously relieve at the global and sub-
297 continental scales except for East Canada, Greenland, Iceland ($1.0\pm0.6 \rightarrow 0.8\pm0.5$) and West
298 North America ($0.9\pm0.3 \rightarrow 0.8\pm0.2$) in the 1.5°C warmer world. In addition, the projected drought
299 severity would also increase in these warmer worlds at the globe ($3.0\pm1.9 \rightarrow 4.5\pm3.0$ and 3.0 ± 1.9
300 $\rightarrow 3.8\pm2.0$ from the baseline period to the 1.5°C and 2°C warmer worlds) and in most regions
301 except for North Asia ($1.8\pm0.6 \rightarrow 1.8\pm0.7$ and $1.8\pm0.6 \rightarrow 1.5\pm0.3$) (Figures 9-10). When global
302 warming is maintained at 1.5°C instead of 2°C above the pre-industrial levels, the drought
303 severity would weaken in most regions except for Sahara ($3.1\pm0.9 \rightarrow 3.5\pm1.3$), North Asia (1.5 ± 0.3
304 $\rightarrow 1.8\pm0.8$), Southeast Asia ($17.2\pm20.1 \rightarrow 35.8\pm57.2$), and West North America ($2.4\pm1.7 \rightarrow$
305 2.5 ± 1.4). The projected uncertainties are relatively low (6~11 models in totally 11 models) for the
306 changes of each drought characteristic in these warming scenarios all over the world, except for
307 some parts of Alaska/Northwest Canada, East Canada, Greenland, Iceland, West North America,
308 Central North America, East North America, Sahara, West Africa, East Africa and North Asia.

309 <Figure 7, here, thanks>

310 <Figure 8, here, thanks>

311 **3.2 Impact of severe drought on population**

312 To understand the societal influences of severe drought, we combine the drought projection with
313 SSP1 population information and estimate the total, urban and rural population affected by
314 severe drought in the baseline period, 1.5°C and 2°C warmer worlds (Figures 11-13). Compared
315 to the baseline period, the frequency of severe drought (PDSI < -3), drought-affected total and
316 urban population would increase in most of the regions in 1.5°C and 2°C warmer worlds. Globally,
317 we estimate that 132.5±216.2 million (350.2±158.8 million urban population and -217.7±79.2
318 million rural population) and 194.5±276.5 million (410.7±213.5 million urban population and
319 -216.2±82.4 million rural population) additional people would be exposed solely to severe
320 droughts in the 1.5°C and 2°C warmer worlds, respectively. The severe drought affected total
321 population would increase under these warming targets in most regions, except for East Asia,
322 North Asia, South Asia, Southeast Asia, Tibetan Plateau and West Coast South America.

323 <Figure 9, here, thanks>

324 <Figure 10, here, thanks>

325 The severe drought affected urban (rural) population would increase (decrease) in all global
326 regions in 1.5°C and 2°C warmer worlds. For example, the projections suggest that more urban
327 population would be exposed to severe drought in Central Europe (10.9±7.7 million), Southern
328 Europe and Mediterranean (14.0±4.6 million), West Africa (65.3±34.1 million), East Asia
329 (16.1±16.0 million), West Asia (16.2±7.4 million) and Southeast Asia (24.4±19.7 million) in 1.5°C
330 warmer world relative to the baseline period. We also find that the number of affected people
331 would escalate further in these regions in 2°C warmer world. In terms of the rural population,
332 less people in Central Asia (-4.1±4.7 million and -3.3±4.1 million for the 1.5°C and 2°C warmer

333 worlds), Central North America (-0.5 ± 1.1 million and -0.4 ± 0.9 million), Southern Europe and
334 Mediterranean (-3.6 ± 3.2 million and -2.9 ± 3.8 million), South Africa (-3.3 ± 1.5 million and -2.9 ± 1.8
335 million), Sahara (-1.0 ± 2.5 million and -0.9 ± 2.9 million), South Asia (-70.2 ± 29.7 million and
336 -72.9 ± 30.0 million), Tibetan Plateau (-2.3 ± 1.8 million and -2.1 ± 1.9 million) and West North
337 America (-1.7 ± 1.0 million and -1.6 ± 1.1 million) would be exposed to the severe drought in
338 1.5°C and 2°C warmer worlds relative to the baseline period. The distinct influences of severe
339 drought on urban and rural population are driven by both climate warming and population
340 growth, especially by the urbanization-induced population migration.

341 <Figure 11, here, thanks>

342 <Figure 12, here, thanks>

343 When global warming approaches 1.5°C (instead of 2°C) above the pre-industrial levels, relatively
344 less total, urban and rural population (except for East Africa and South Asia) would be affected
345 despite more frequent severe drought in most regions such as East Asia, Southern Europe and
346 Mediterranean, Central Europe and Amazon. This implies that the benefit of holding global
347 warming at 1.5°C instead of 2°C is apparent to the severe-drought affected total, urban and rural
348 population in most regions, but challenges remain in East Africa and South Asia.

349 <Figure 13, here, thanks>

350 **4 Discussions**

351 The changes in PDSI, drought duration, intensity and severity with climate warming (i.e., 1.5°C
352 and 2°C warmer worlds) projected in this study is in general agreement with that concluded by
353 IPCC (2013) despite regional variation. For example, as revealed in this study, the gradual decline
354 of PDSI (drought-prone) in American Southwest and Central Plains was also projected using an

355 empirical drought reconstruction and soil moisture metrics from 17 state-of-the-art GCMs in the
356 21st century (Cook et al., 2015). The ascending risk of drought in Sahara, North Australia and
357 South Africa coincided with Huang et al. (2017), which projected that global drylands would
358 degrade in 2°C warmer world. Moreover, the increases in drought duration, intensity and severity
359 in Central America, Amazon, South Africa and Mediterranean are in agreement with the
360 extension of dry spell length and less water availability in these regions under the 1.5°C and/or
361 2°C warming scenarios (Schleussner et al., 2016; Lehner et al., 2017). In addition, we find that the
362 affected population attributes more (50%~75%) to the population growth rather than the climate
363 change driven severe drought in the 1.5°C and 2°C warmer worlds. This number is greater than
364 that concluded by Smirnov et al. (2016), maybe due to different study periods, population data,
365 drought index and warming scenarios used.

366

367 Projections presented in current study inherited several sources of uncertainty. Firstly, there are
368 considerable uncertainties in the numerical projections from different climate models under
369 varied greenhouse gas emission scenarios, especially on a regional scale (i.e., Sahara,
370 Alaska/Northwest Canada and North Asia). However, the utility of multiple GCMs and emission
371 scenarios should allow us to synthesize future projections better than single model/scenario
372 analysis (Schleussner et al., 2016; Wang et al., 2017; Lehner et al., 2017). On top of that, we
373 performed uncertainty analysis such as understanding the model consistency (e.g.,
374 increase/decrease) and inter-model variance (for magnitude changes). These enable us to
375 characterize regional and global projections which could vary due to different model structure of
376 GCMs and how they behave under different RCP scenarios. Moreover, the global and regional

377 responses (i.e., warming/precipitation patterns) to varied warming scenarios (i.e., 1.5°C and 2°C)
378 showed little dependences on RCP scenarios (King et al., 2017; Hu et al., 2017). Therefore, the
379 uncertainty caused by the choice of RCP scenarios might be small. Secondly, there are various
380 ways of picking the 1.5°C or 2°C warming signals (King et al., 2017). Current study considered
381 both the influences of multi-model and multi-scenario for each warming scenario using the
382 20-year smoothed multi-model ensemble mean GMT. The selected periods of 1.5°C and 2.0°C
383 warmer worlds are close to that of King et al. (2017). Finally, the SSP1 population data and the
384 single drought index used might introduce uncertainties. Despite these sources of uncertainty,
385 these projections are quite robust with high model consistency across most regions.

386

387 This analysis evaluated the risk of droughts in terms of how they would change in the future
388 period (1.5°C or 2°C warmer worlds) relative to the baseline period; and the difference between
389 the two warmer worlds. In this perspective, uncertainty arises from climate model bias in
390 between two periods more or less cancels each other. Previous studies demonstrated that
391 bias-corrections do not yield much difference in such circumstance (e.g., Sun et al., 2011; Maraun,
392 2016). In addition, the methodology here requires the meteorological information with physical
393 meaning (see Section 2.1) that is consistent with the energy balance of the climate model
394 (Equation 3 in Section 2.3), hence existing bias-correction measures (with known weakness in
395 maintaining the physical aspect of bias-corrected output) appears less feasible. (Future
396 innovation which accounts for both statistics and energy balance of climate model output in new
397 bias-correction methodology for handling the highly non-linear outcomes should be a subject of
398 scientific interest.) The rationale of using model consistency (Figures 3, 5, 7, 9) as a form of

399 “confidence index” here emerges from the idea that, whilst model validation in historical period
400 is helpful, it does not necessary reveal the ability of each climate model in projection of risk
401 change. Thus this kind of confidence index is informative for synthesizing multi-model projections,
402 probably explains why it is still common in many global studies involving multi-model ensembles
403 (e.g., Hirabayashi et al., 2013; Koirala et al., 2014).

404

405 **5 Conclusions**

406 Motivated by the 2015 Paris Agreement proposal, we analyzed the CMIP5 GCM output and
407 presented the first comprehensive assessment of changes in drought characteristics and the
408 potential impacts of severe drought on population (total, urban and rural) in 1.5°C and 2°C
409 warmer worlds. We found that the risk of drought would increase (i.e., decrease in PDSI, increase
410 in drought duration, drought intensity and drought severity) globally and most regions (i.e.,
411 Amazon, Northeastern Brazil, Central Europe) for in 1.5°C and 2°C warmer worlds relative to the
412 baseline period (1986-2005). However, the amplitudes of change in drought characteristics vary
413 among the regions. Relative to the 2°C warming target, a 1.5°C warming target is more likely to
414 reduce drought risk (less drought duration, drought intensity and drought severity but relatively
415 more frequent severe drought) significantly on both global and regional scales. The high model
416 consistency (6~11 out of 11 GCMs) across most regions (especially Amazon, Sahara and
417 Northeastern Brazil) gives us more confidence on these projections.

418

419 Despite the uncertainties inherited from the GCMs and population data used, as well as the
420 definition of the 1.5°C and 2°C periods, we found significant changes of drought characteristics

421 under both warming scenarios and societal impacts of severe drought by limiting temperature
422 target at 1.5 °C instead of 2 °C in several hotspot regions. More total (+132.5±216.2 million and
423 +194.5±276.5 million globally) and urban population (+350.2±158.8 million and +410.7±213.5
424 million globally) would be exposed to severe drought in most regions (especially East Africa, West
425 Africa and South Asia) in 1.5 °C and 2 °C warmer worlds, particularly for the latter case.

426

427 Meanwhile, less rural population (-217.7±79.2 million and -216.2±82.4 million globally) in, e.g.,
428 Central Asia, East Canada, Greenland, Iceland, Central North America, Southern Europe and
429 Mediterranean, North Australia, South Africa, Sahara, South Asia, Tibetan Plateau and West
430 North America would be affected. When global mean temperature increased by 1.5 °C instead of
431 2 °C above the pre-industrial level, the total, urban and rural population affected by severe
432 drought would decline in most regions except for East Africa and South Asia.

433

434 In general, this comprehensive global drought risk assessment should provide useful insights for
435 international decision-makers to develop informed climate policy within the framework of the
436 2015 Paris Agreement. Whilst most regions would benefit from reduced societal impacts in the
437 1.5 °C warmer world, local governments in East Africa and South Asia should be prepared to deal
438 with drought-driven challenges (see paragraph above). Future studies on understanding the
439 causes of changes in global and regional droughts (e.g., changing pattern/duration of
440 precipitation and evaporative demand) with respect to these warming targets should assist
441 drought risk adaptation and mitigation planning.

442

443 **Data availability.** The datasets applied in this study are available at the following locations:

444 — CMIP5 model experiments (Taylor et al., 2012), [https://esgf-data.dkrz.de/projects/](https://esgf-data.dkrz.de/projects/esgf-dkrz/)
445 [esgf-dkrz/](https://esgf-data.dkrz.de/projects/esgf-dkrz/)

446 — Spatial population scenarios (Shared Socioeconomic Pathway 1, SSP1, Jones and O’Niell,
447 2016), <https://www2.cgd.ucar.edu/sections/tss/iam/spatial-population-scenarios>

448 **Competing interests.** The authors declare that they have no conflict of interest.

449 **Acknowledgements.** This study was financially supported by the National Research and
450 Development Program of China (2016YFA0602402 and 2016YFC0401401), the Key Research
451 Program of the Chinese Academy of Sciences (ZDRW-ZS-2017-3-1), the CAS Pioneer Hundred
452 Talents Program (Fubao Sun) and the CAS President’s International Fellowship Initiative (Wee Ho
453 Lim, 2017PC0068). We thank the Editor (Michel Crucifix), Dimitri Defrance and an anonymous
454 reviewer for their helpful comments.

455

456 **References**

457 Aghakouchat, A., Cheng L., Mazdidasni, O., and Farahmand, A.: Global warming and changes in
458 risk of concurrent climate extremes: insights from the 2014 California drought, *Geophys. Res.*
459 *Lett.*, 41, 8847-8852, doi:10.1002/2014GL062308, 2015.

460 Allen, R., Pereira, L.S., Raes, D., and Smith, M.: Crop evapotranspiration guidelines for computing
461 crop water requirements-FAO Irrigation and drainage paper 56, FAO-Food and Agriculture
462 Organization of the United Nations, Rome, 1998.

463 Ault, T.R., Mankin, J.S., Cook, B.I., and Smerdon, J.E.: Relative impacts of mitigation, temperature,
464 and precipitation on 21st-century megadrought risk in the American Southwest, *Sci. Adv.*, 2, 1-9,
465 doi:10.1126/sciadv.1600873, 2016.

466 Ayantobo, O.O., Li, Y., Song, S.B., and Yao, N.: Spatial comparability of drought characteristics and
467 related return periods in mainland China over 1961-2013, *J. Hydrol.*, 550, 549-567,
468 doi:10.1016/j.jhydrol.2017.05.019, 2017.

469 Cheng, L., Hoerling, M., Aghakouchak, A., Livneh, B., Quan, X.W., and Eischeid, J.: How has
470 human-induced climate change affected California drought risk? *J. Clim.*, 29, 111-120,
471 doi:10.1175/JCLI-D-15-0260.1, 2016.

472 Cook, B.I., Ault, T.R., Smerdon, J.E.: Unprecedented 21st century drought risk in the American
473 Southwest and Central Plains, *Sci. Adv.*, 1, e1400082, 2015.

474 Cuaresma, J.: SSP economic growth projections: IIASA model. In supplementary note for the SSP
475 data sets.
476 https://secure.iiasa.ac.at/web-apps/ene/SspDb/static/download/ssp_supplementary%20text.pdf
477 [f](#), 2012.

478 Dai, A.G.: Characteristics and trends in various forms of the Palmer drought severity index during
479 1900-2008, *J. Geophys. Res.*, 116, D12115, doi: 10.1029/2010JD015541, 2011.

480 Dai, A.G.: Increasing drought under global warming in observations and models, *Nat. Clim.*
481 *Change*, 3, 52-58, doi: 10.1038/NCLIMATE1633, 2012.

482 Fischer, E.M., Beyerle, U., and Knutti, R.: Robust spatially aggregated projections of climate
483 extremes, *Nat. Clim. Change*, 2, 1033-1038, doi:10.1038/nclimate2051, 2013.

484 Fu, Q., and Feng, S.: Responses of terrestrial aridity to global warming, *J. Geophys. Res.*, 119,
485 7863-7875, doi: 10.1002/2014JD021608, 2014.

486 Hao, Z.C., Singh, V.P., Xia, Y.L.: Seasonal drought prediction: advances, challenges, and future
487 prospects. *Rev. Geophys.*, 56, doi: 10.1002/2016/RG000549.

488 Heim Jr. R.R.: A review of twentieth-century drought indices used in the United States, *BAMS*,
489 1149-1165.

490 Hirabayashi, Y., Mahendran, R., Korala, S., Konoshima, L., Yamazaki, D., Watanabe, S., Kim, H. and
491 Kanae, S.: Global flood risk under climate change, *Nat. Clim. Change*, 3, 816-821, doi:
492 10.1038/nclimate1911, 2013.

493 Hu, T., Sun, Y., and Zhang, X.B.: Temperature and precipitation projection at 1.5 and 2°C increase
494 in global mean temperature (in Chinese), *Chin. Sci. Bull.*, 62, 3098-3111, doi:
495 10.1360/N972016-01234, 2017.

496 Hulme, M.: 1.5°C and climate research after the Paris Agreement, *Nat. Clim. Change*, 6, 222-224,
497 doi:10.1038/nclimate2939, 2016.

498 IPCC: Managing the Risks of Extreme Events and Disasters to Advance Climate Change Adaptation,
499 in: A Special Report of Working Group I and II of the Intergovernmental Panel on Climate
500 Change, edited by: Field, C.B., Barros, V., Stocker, T.F., Qin, D., Dokken, D.J., Ebi, K.L.,
501 Mastrandrea, M.D., Mach, K.J., Plattner, G.-K., Allen, S.K., Tignor, M., and Midgley, P.M.,
502 Cambridge University Press, Cambridge, UK and New York, NY, USA, 582 pp, 2012.

503 IPCC: Summary for Policymakers, in: *Climate Change 2013: The Physical Science Basis*,
504 Contribution of Working Group I to the Fifth Assessment Report of the Intergovernmental
505 Panel on Climate Change, edited by: Stocker, T., Qin, D., Plattner, G.-K., Tignor, M., Allen, S.,

506 Boschung, J., Nauels, A., Xia, Y., Bex, V., and Midgley, P., IPCC AR WGI, Cambridge University
507 Press, Cambridge, UK and New York, NY, USA, 1-100, 2013.

508 Jacobi, J., Perrone, D., Duncan, L.L., and Hornberger, G.: A tool for calculating the Palmer drought
509 indices, *Water Resour. Res.*, 49, 6086-6089, doi: 10.1002/wrcr.20342, 2013.

510 James, R., Washington, R., Schleussner, C.-F., Rogelj, J., and Conway, D.: Characterizing
511 half-a-degree difference: a review of methods for identifying regional climate responses to
512 global warming target, *WIREs Clim. Change*, 8, e457, doi: 10.1002/wcc.457, 2017.

513 Jones, B. and O'Neill, B.C.: Spatially explicit global population scenarios consistent with the
514 Shared Socioeconomic Pathways, *Environ. Res. Lett.*, 11, 084003,
515 <http://iopscience.iop.org/1748-9326/11/8/084003>, 2016.

516 Kelley, C.P., Mohtadi, S., Cane, M.A., Seager, R., and Kushnir, Y.: Climate change in the Fertile
517 Crescent and implications of the recent Syrian drought, *Proc. Natl. Acad. Sci.*, 112, 3241-3246,
518 doi: 10.1073/pnas.1421533112, 2015.

519 Kiem, A.S., Johnson, F., Westra, S., van Dijk, A., Evans, J.P., O'Donnell, A., Rouillard, A., Barr, C.,
520 Tyler, J., Thyer, M., Jakob, D., Woldemeskel, F., Sivakumar, B., Mehrotra, R.: Nature hazards in
521 Australia: drought, *Clim. Change*, 139, 37-54, doi:10.1007/s10584-016-1798-7, 2016.

522 King, A.D., Karoly, D.J., and Henley, B.J.: Australian climate extremes at 1.5°C and 2°C of global
523 warming, *Nat. Clim. Change*, 7, 412-416, doi:10.1038/nclimate3296, 2017.

524 Koirala, S., Hirabayashi, Y., Mahendran, R., and Kanae, S.: Global assessment of agreement among
525 streamflow projections using CMIP5 model outputs, *Environ. Res. Lett.*, 9, 064017(11pp), 2014.

526 Lehner, F., Coats, S., Stocker, T.F., Pendergrass, A.G., Sanderson, B.M., Paible, C.C., and Smerdon,
527 J.E.: Projected drought risk in 1.5°C and 2°C warmer climates, *Geophys. Res. Lett.*, 44,
528 7419-7428, doi:10.1002/2017GL074117, 2017.

529 Liu, W.B. and Sun, F.B.: Assessing estimates of evaporative demand in climate models using
530 observed pan evaporation over China, *J. Geophys. Res. Atmos.*, 121, 8329-8349, doi:
531 10.1002/2016JD025166, 2016.

532 Liu, W.B. and Sun, F.B.: Projecting and attributing future changes of evaporative demand over
533 China in CMIP5 climate models, *J. Hydrometeor.*, 18, 977-991, doi: 10.1175/JHM-D-16-0204.1,
534 2017.

535 Liu, W.B., Wang, L., Chen, D.L., Tu, K., Ruan, C.Q., and Hu, Z.Y.: Large-scale circulation classification
536 and its links to observed precipitation in the eastern and central Tibetan Plateau, *Clim. Dyn.*,
537 46(11-12), 3481-3497, doi: 10.1007/s00382-015-2782-z, 2016.

538 Lyon, B.: Seasonal drought in the Greater Horn of Africa and its recent increase during the
539 march-may long rains, *J. Clim.*, 27, 7953-7975, doi:10.1175/JCLI-D-13-00459.1, 2014.

540 Maraun, D.: Bias correcting climate change simulations – a critical review, *Curr. Clim. Change Rep.*,
541 2, 211-220, 2016.

542 Masih, I., Maskey, S., Mussá, F.E.F., and Trambauer, P.: A review of droughts on the African
543 continent: a geospatial and long-term perspective, *Hydrol. Earth Syst. Sci.*, 18, 3635-3649,
544 doi:10.5149/hess-18-3635-2014, 2014.

545 McKee, T.B., Doesken, N.J. and Kleist, J.: The relationship of drought frequency and duration of
546 time scales, Eighth Conference on Applied Climatology, American Meteorological Society, Jan
547 17-23, Anaheim CA, PP. 179-186, 1993.

548 Mishra, A.K. and Singh, V.P.: A review of drought concepts, *J. Hydrol.*, 291, 201-216,
549 doi:10.1016/j.jhydrol.2010.07.012, 2010.

550 Mitchell, D., James, R., Forster, P.M., Betts, R.A., Shiogama, H., and Allen, M.: Realizing the
551 impacts of a 1.5°C warmer world, *Nat. Clim. Change*, 6, 735-737, doi:10.10038/nclimate3055,
552 2016.

553 Mitchell, D., AchutaRao, K., Allen, M., Bethke, I., Beyerle, U., Ciavarella, A., Forster, P.M.,
554 Fuglestvedt, J., Gillett, N., Hausteine, K., Ingram, W., Iversen, T., Kharin, V., Klingaman, N.,
555 Massey, N., Fischer, E., Schleussner, C.-F., Scinocca, J., Seland, Ø., Shiogama, H., Shuckburgh, E.,
556 Sparrow, S., Stone, D., Uhe, P., Wallom, D., Wehner, M., and Zaaboul, R.: Half a degree
557 additional warming, prognosis and projected impacts (HAPPI): background and experimental
558 design, *Geosci. Model Dev.*, 10, 571-583, doi:10.5194/gmd-10-571-2017,2017.

559 O’Niell, B.C., Tebaldi, C., van Vuuren, D.P., Eyring, C., Friedlingstein, P., Hurtt, G., Knutti, R., Kriegler,
560 E., Lamarque, J.-F., Lowe, J., Meehl, G.A., Moss, R., Riahi, K., and Sanderson, B.M.: The Scenario
561 Model Intercomparison Project (ScenarioMIP) for CMIP6, *Geosci. Model Dev.*, 9, 3461-3482,
562 doi:10.5194/gmd-9-3461-2016, 2016.

563 Palmer, W.C.: Meteorological drought, U.S. Department of Commerce Weather Bureau Research,
564 Paper 45, 58 pp., 1965.

565 Peters, G.P.: The “best available science” to inform 1.5°C policy choice, *Nat. Clim. Change*, 6,
566 646-649, doi: 10.1038/nclimate3000, 2016.

567 Qiu, J.: China drought highlights future climate threats, *Nature*, 465, 142-143,
568 doi:10.1038/465142a, 2010.

569 Sanderson, B.M., Xu, Y.Y., Tebaldi, C., Wehner, M., O'Neill, B., Jahn, A., Pendergrass, A.G., Lehner,
570 F., Strand, W.G., Lin, L., Knutti, R. and Lamarque, J.F.: Community climate simulations to assess
571 avoided impact in 1.5°C and 2°C futures, *Earth Syst. Dyn. Discuss.*, doi:10.5194/esd-2017-42,
572 2017.

573 Schleussner, C., Lissner, T.K., Fischer, E.M., Wohland, J., Perrette, M., Golly, A., Rogelj, J., Childers,
574 K., Schewe, J., Frieler, K., Mengel, M., Hare, W., and Schaeffer, M.: Differential climate impacts
575 for policy-relevant limits to global warming: the case of 1.5°C and 2°C, *Earth Syst. Dynam.*, 7,
576 327-351, doi: 10.5194/esd-7-327-2016, 2016.

577 Sheffield, J., Wood, E.F., and Roderick, M.L.: Little change in global drought over the past 60 years,
578 *Nature*, 491, 435-439, doi:10.1038/nature11575, 2012.

579 Smirnov, O., Zhang, M.H., Xiao, T.Y., Orbell, J., Lobben, A., and Gordon, J.: The relative importance
580 of climate change and population growth for exposure to future extreme droughts, *Clim.*
581 *Change*, 138, 1-2, 41-53, doi: 10.1007/s10584-016-1716-z, 2016.

582 Sun, F., Roderick, M.L., Lim, W.H., and Farquhar, G.D.: Hydroclimatic projections for the
583 Murray-Darling Basin based on an ensemble derived from Intergovernmental Panel on Climate
584 Change AR4 climate models, *Water Resour. Res.*, 47, W00G02, doi: 10.1029/2010WR009829,
585 2011.

586 Taylor, L.E., Stouffer, R.J., and Meehl, G.A.: An Overview of CMIP5 and the Experiment Design, *B.*
587 *Am. Meteorol. Soc.*, <https://doi.org/10.1175/BAMS-D-11-00094.1>, 2012.

588 UNFCCC Conference of the Parties: Adoption of the Paris Agreement, *FCCC/CP/2015/10Add.1*,
589 1-32, Paris, 2015.

590 Van Dijk, A.I.J.M., Beck, H.E., Crosbie, R.S., de Jeu, A.M., Liu, Y.Y., Podger, G.M., Timbal, B., and
591 Viney, N.R.: The Millennium Drought in southeast Australia (2001-2009): Natural and human
592 causes and implications for water resources, ecosystems, economy, and society, *Water Resour.*
593 *Res.*, 49, 1040-1057, doi:10.1002/wrcr.20123, 2013.

594 Van Vuuren, D.P., Stehfest, E., Gernaat, D.E.H.J., Doelman, J.C., van den Berg, M., Harmsen, M., de
595 Boer, H.S., Bouwman, L.F., Daioglou, V., Edelenbosch, O.Y., Girod, B., Kram, T., Lassaletta, L.,
596 Lucas, P.L., van Meijl, H., Müller, C., van Ruijven, B.J., van der Sluis, S., and Tabeau, A.: Energy,
597 land-use and greenhouse gas emissions trajectories under a green growth paradigm, *Global*
598 *Environ. Chang.*, 42, 237-250, doi: 10.1016/j.gloenvcha.2016.05.008, 2017.

599 Wang, A.H., Lettenmaier, and D.P., Sheffield, J.: Soil moisture drought in China, 1950-2006, *J.*
600 *Climate*, 24, 3257-3271, doi: 10.1175/2011JCLI3733.1, 2011.

601 Wang, Z.L., Lin, L., Zhang, X.Y., Zhang, H., Liu, L.K., and Xu, Y.Y.: Scenario dependence of future
602 changes in climate extremes under 1.5°C and 2°C global warming, *Sci. Rep.*, 7:46432,
603 doi:10.1038/srep46432, 2017.

604 Wells, N., Goddard, S., Hayes, M.J.: A self-calibrating palmer drought severity index, *J. Clim.*, 17,
605 2335-2351, 2004.

606 Yevjevich, V., and Ingenieur, J.: An objective approach to definitions and investigations of
607 continental hydrological drought, *Water Resource Publ.*, Fort Collins, 1967.

608 Zargar, A., Sadiq, R., Naser, B., Khan, F.I.: A review of drought indices, *Environ. Rev.*, 19, 333-349.

609 Zhang, J., Sun, F.B., Xu, J.J., Chen, Y.N., Sang, Y.-F., and Liu, C.M.: Dependence of trends in and
610 sensitivity of drought over China (1961-2013) on potential evaporation model, *Geophys. Res.*
611 *Let.*, 43, 206-213, doi: 10.1002/2015GL067473, 2016.

612 Zuo, D.D., Hou, W., and Wang, W.X.: Sensitivity analysis of sample number of the drought
613 descriptive model built by Copula function in southwest China, *Acta Phys. Sin.*, 64(10), 100203,
614 doi:10.7498/aps.64.100203,2015
615

616 **Table 1:** Details of CMIP5 climate models applied in this study

617

Climate models	abbreviation	Horizontal Resolution	Future Scenarios
ACCESS1.0	ACCESS	1.300×1.900 degree	RCP4.5, RCP8.5
BCC_CSM1.1	BCC	2.813×2.791 degree	RCP4.5, RCP8.5
BNU-ESM	BNU	2.810×2.810 degree	RCP4.5, RCP8.5
CanESM23	CANESM	2.813×2.791 degree	RCP4.5, RCP8.5
CNRM-CM5	CNRM	1.406×1.401 degree	RCP4.5, RCP8.5
CSIRO Mk3.6.0	CSIRO	1.875×1.866 degree	RCP4.5, RCP8.5
GFDL CM3	GFDL	2.500×2.000 degree	RCP4.5, RCP8.5
INM-CM4.0	INM	2.000×1.500 degree	RCP4.5, RCP8.5
IPSL-CM5B-LR	IPSL	1.875×3.750 degree	RCP4.5, RCP8.5
MRI-CGCM3	MRI	1.125×1.125 degree	RCP4.5, RCP8.5
MIROC-ESM	MIROC	2.813×2.791 degree	RCP4.5, RCP8.5

618 **Table 2:** Definition of regions in this study, after IPCC (2012)

619

620

ID	abbreviation	Regional Representation
1	ALA	Alaska/Northwest Canada
2	CGI	East Canada, Greenland, Iceland
3	WNA	West North America
4	CNA	Central North America
5	ENA	East North America
6	CAM	Central America and Mexico
7	AMZ	Amazon
8	NEB	Northeastern Brazil
9	WSA	West Coast South America
10	SSA	Southeastern South America
11	NEU	Northern Europe
12	CEU	Central Europe
13	MED	Southern Europe and Mediterranean
14	SAH	Sahara
15	WAF	West Africa
16	EAF	East Africa
17	SAF	Southern Africa
18	NAS	North Asia
19	WAS	West Asia
20	CAS	Central Asia
21	TIB	Tibetan Plateau
22	EAS	East Asia
23	SAS	South Asia
24	SEA	Southeast Asia
25	NAU	North Australia
26	SAU	South Australia/New Zealand
27	GLOBE	Globe

621 **Figure captions:**

622 **Figure 1:** Definition of the baseline period, 1.5°C and 2°C warmer worlds based on CMIP5
623 GCM-simulated changes in global mean temperature (GMT, relative to the pre-industrial levels:
624 1850-1900). The dark blue and dark yellow shadows indicate the 25th and 75th percentiles of
625 multi-model simulated GMT for RCP 4.5 and RCP 8.5 scenarios, respectively. Both the
626 multi-model ensemble mean and percentiles shown in the figure are smoothed using a moving
627 average approach in a 20-year window

628

629 **Figure 2:** Palmer Drought Severity Index (PDSI)-based drought characteristics definition through
630 the run theory

631

632 **Figure 3:** Changes in multi-model ensemble mean PDSI (i) and model consistency (ii) on a spatial
633 resolution of $0.5^\circ \times 0.5^\circ$, (a) from the baseline period to 1.5°C warmer world, (b) from the
634 baseline period to 2°C warmer world and (c): (a)-(b). Robustness of projections increases with
635 higher model consistency and vice-versa. The dark-gray boxes show the world regions adopted by
636 IPCC (2012), which are labeled in (a)(i) using the ID numbers defined in Table 2. Legend in (a)(i)
637 applies to (b)(i) and (c)(i); legend in (a)(ii) applies to (b)(ii) and (c)(ii).

638

639 **Figure 4:** Multi-model projected PDSI at the globe (66°N - 66°S) and in 27 world regions for the
640 baseline period, 1.5°C and 2°C warmer worlds. The projected uncertainty of multiple climate
641 models is shown through box plots for each region and for each period

642

643 **Figure 5:** Changes in multi-model ensemble mean drought duration (months) (i) and model
644 consistency (ii) on a spatial resolution of $0.5^\circ \times 0.5^\circ$, (a) from the baseline period to 1.5°C warmer
645 world, (b) from the baseline period to 2°C warmer world and (c) : (a)-(b). The dark-gray boxes
646 show the regions adopted by IPCC (2012), which are labeled in (a)(i) using the ID numbers
647 defined in Table 2. Legend in (a)(i) applies to (b)(i) and (c)(i); legend in (a)(ii) applies to (b)(ii) and
648 (c)(ii).

649

650 **Figure 6:** Multi-model projected drought duration (months) at the globe (66°N - 66°S) and in 27
651 world regions for the baseline period, 1.5°C and 2°C warmer worlds. The projected uncertainty of
652 multiple climate models is shown through box plots for each region and for each period

653

654 **Figure 7:** Changes in multi-model ensemble mean drought intensity (dimensionless) (i) and model
655 consistency (ii) on a spatial resolution of $0.5^\circ \times 0.5^\circ$, (a) from the baseline period to 1.5°C warmer
656 world, (b) from the baseline period to 2°C warmer world and (c): (a)-(b). The dark-gray boxes
657 show the regions adopted by IPCC (2012), which are labeled in (a)(i) using the ID numbers
658 defined in Table 2. Legend in (a)(i) applies to (b)(i) and (c)(i); legend in (a)(ii) applies to (b)(ii) and
659 (c)(ii).

660

661 **Figure 8:** Multi-model projected drought intensity (dimensionless) at the globe (66°N - 66°S) and in
662 27 world regions for the baseline period, 1.5°C and 2°C warmer worlds. The projected uncertainty
663 of multiple climate models is shown through box plots for each region and for each period

664

665 **Figure 9:** Changes in multi-model ensemble mean drought severity (dimensionless) (i) and model
666 consistency (ii) on a spatial resolution of $0.5^\circ \times 0.5^\circ$, (a) from the baseline period to 1.5°C warmer
667 world, (b) from the baseline period to 2°C warmer world and (c): (a)-(b). The dark-gray boxes
668 show the regions adopted by IPCC (2012), which are labeled in (a)(i) using the ID numbers
669 defined in Table 2. Legend in (a)(i) applies to (b)(i) and (c)(i); legend in (a)(ii) applies to (b)(ii) and
670 (c)(ii).

671

672 **Figure 10:** Multi-model projected drought severity (dimensionless) at the globe (66°N - 66°S) and
673 in 27 world regions for the baseline period, 1.5°C and 2°C warmer worlds. The projected
674 uncertainty of multiple climate models is shown through box plots for each region and for each

675 period

676

677 **Figure 11:** Multi-model projected frequency (Freq.) and affected total population (Pop., million)
678 of severe drought (PDSI < -3) at the globe and in 27 world regions for the baseline period (black,
679 fixed SSP1 2000 population), 1.5°C (orange, fixed SSP1 2100 population) and 2°C (red, fixed SSP1
680 2100 population) warmer worlds. The projected uncertainties (standard deviation of
681 multiple-model results) of multiple climate models are shown by error bars (horizontal and
682 vertical)

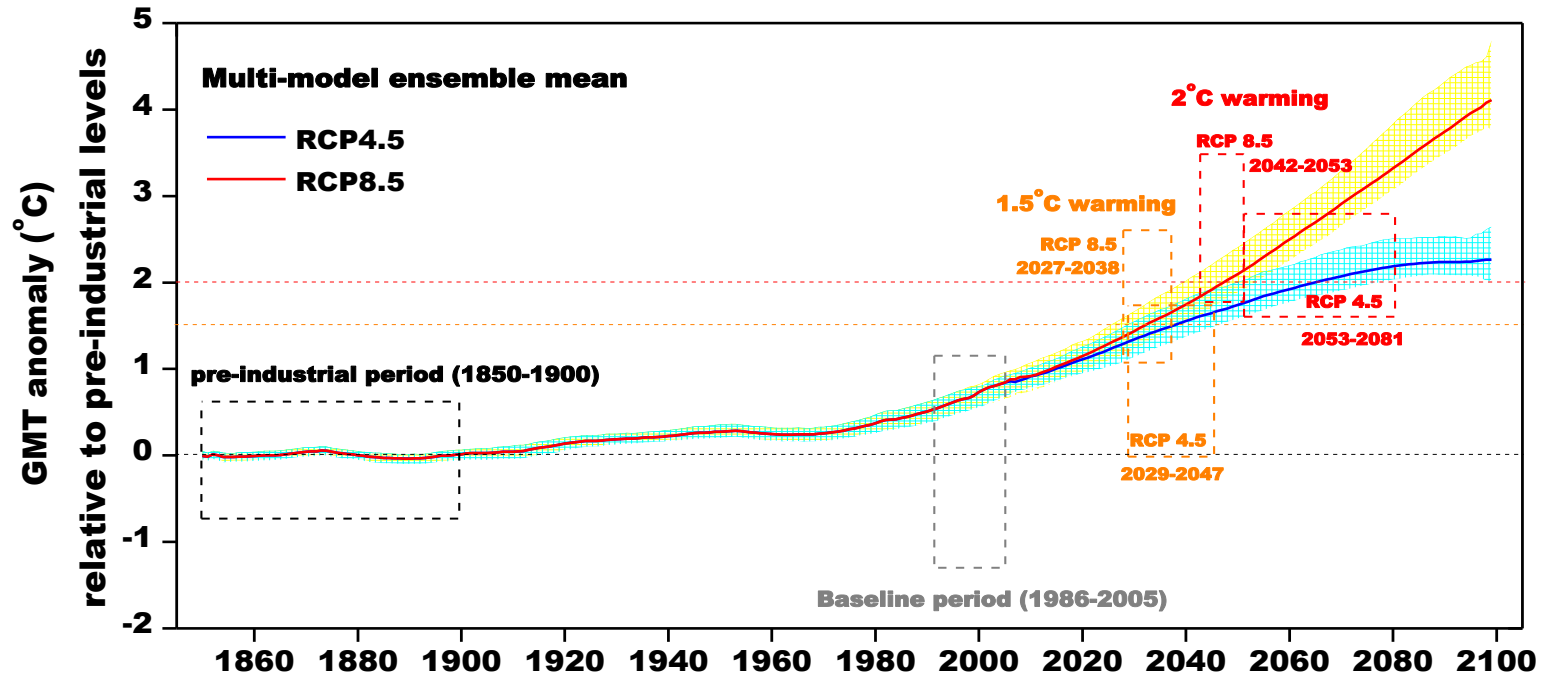
683

684 **Figure 12:** Multi-model projected frequency (Freq.) and affected urban population (Pop., million)
685 of severe drought (PDSI < -3) at the globe and in 27 regions for the baseline period (black, fixed
686 SSP1 2000 population), 1.5°C (orange, fixed SSP1 2100 population) and 2°C (red, fixed SSP1 2100
687 population) warmer worlds. The projected uncertainties (standard deviation of multiple-model
688 results) of multiple climate models are shown by error bars (horizontal and vertical)

689

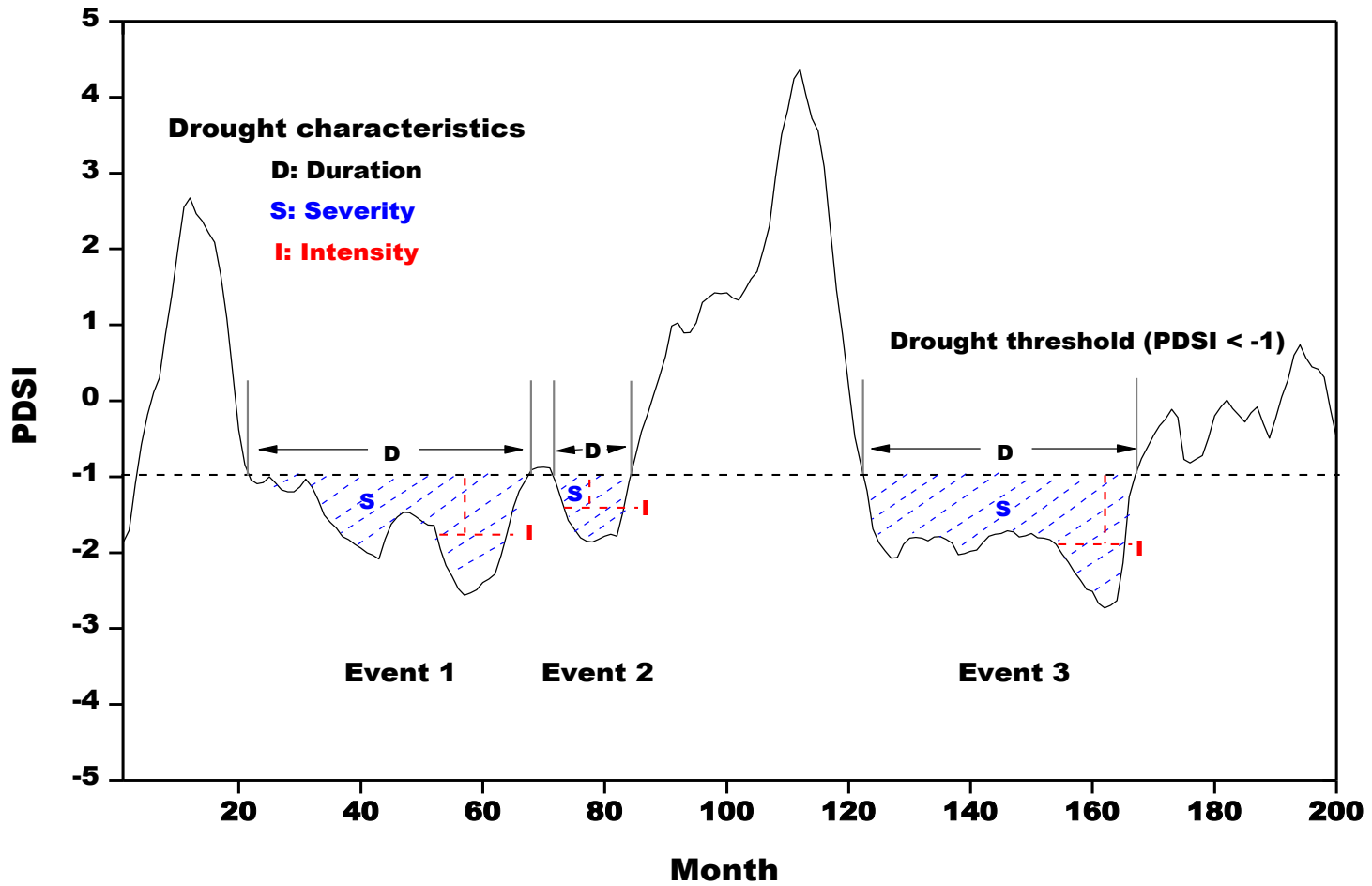
690 **Figure 13:** Multi-model projected frequency (Freq.) and affected rural population (Pop., million)
691 of severe drought (PDSI < -3) at the globe and in 27 regions for the baseline period (black, fixed
692 SSP1 2000 population), 1.5°C (orange, fixed SSP1 2100 population) and 2°C (red, fixed SSP1 2100
693 population) warmer worlds. The projected uncertainties (standard deviation of multiple-model
694 results) of multiple climate models are shown by error bars (horizontal and vertical)

695 **Figure 1:** Definition of the baseline period, 1.5°C and 2°C warmer worlds based on CMIP5 GCM-simulated changes in global mean temperature
696 (GMT, relative to the pre-industrial levels: 1850-1900). The dark blue and dark yellow shadows indicate the 25th and 75th percentiles of
697 multi-model simulated GMT for RCP 4.5 and RCP 8.5 scenarios, respectively. Both the multi-model ensemble mean and percentiles shown in
698 the figure are smoothed using a moving average approach in a 20-year window
699



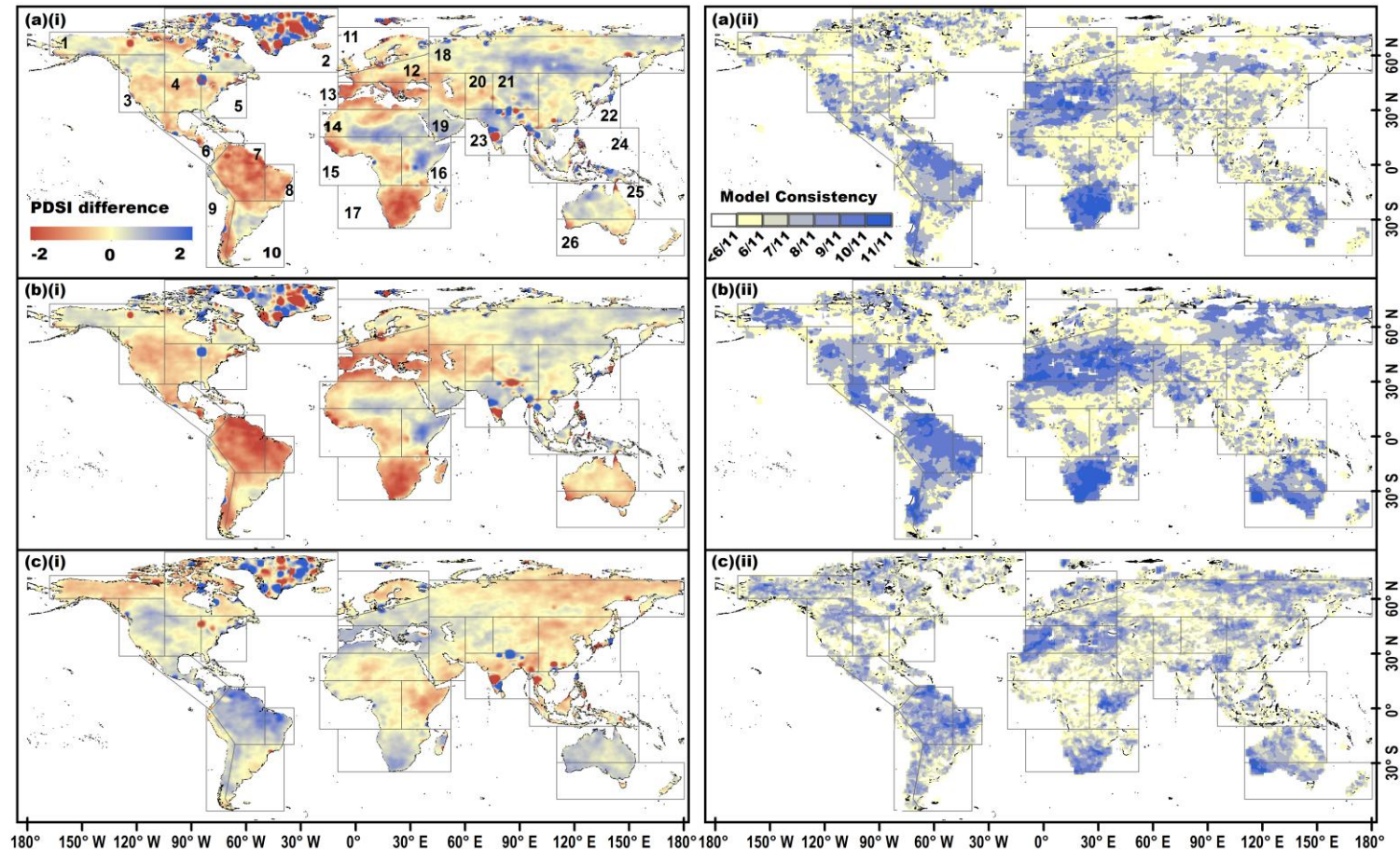
700
701

702 **Figure 2:** Palmer Drought Severity Index (PDSI)-based drought characteristics definition through the run theory



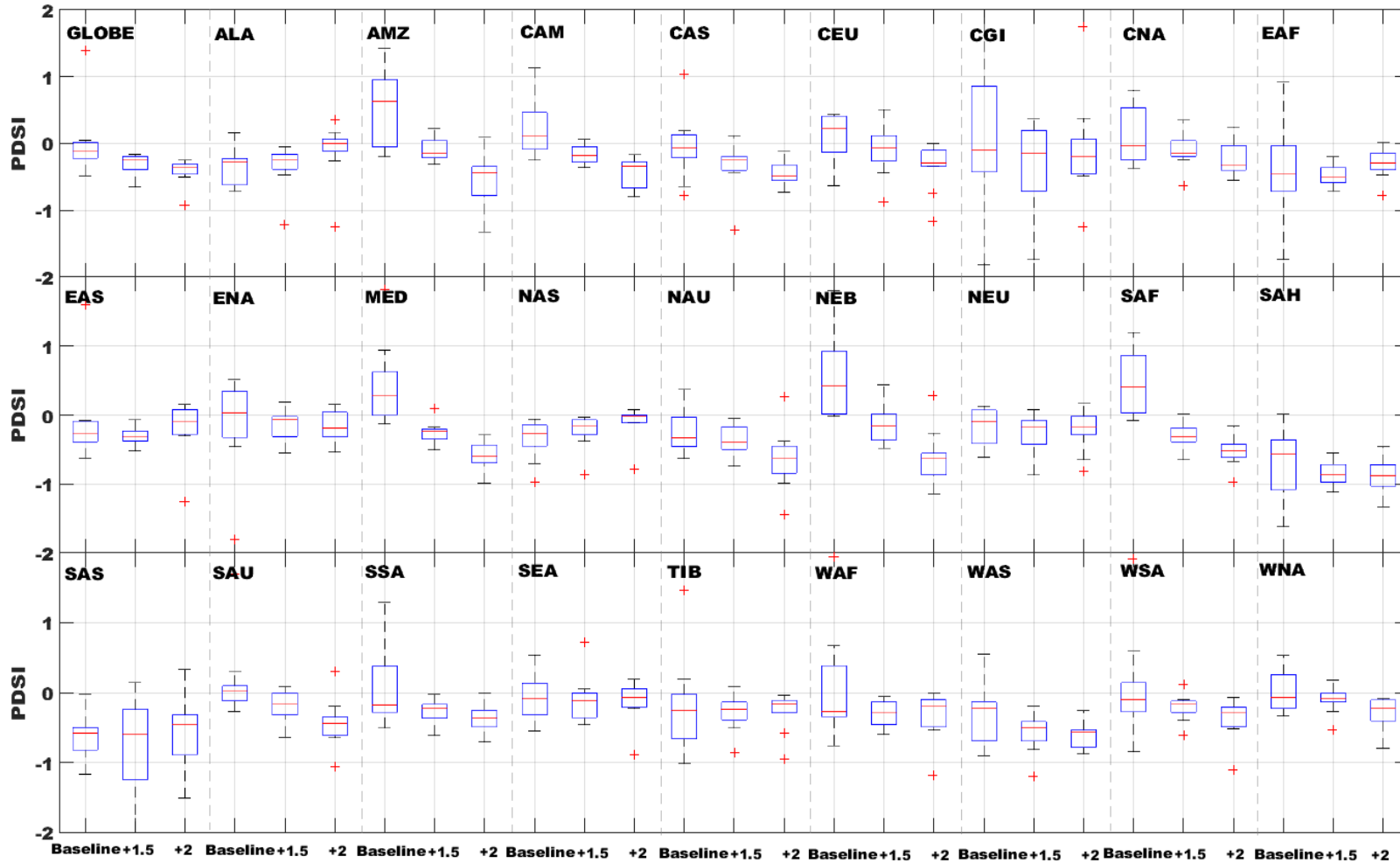
703
704

705 **Figure 3:** Changes in multi-model ensemble mean PDSI (i) and model consistency (ii) on a spatial resolution of $0.5^\circ \times 0.5^\circ$, (a) from the baseline
 706 period to 1.5°C warmer world, (b) from the baseline period to 2°C warmer world and (c): (a)-(b). Robustness of projections increases with
 707 higher model consistency and vice-versa. The dark-gray boxes show the world regions adopted by IPCC (2012), which are labeled in (a)(i) using
 708 the ID numbers defined in Table 2. Legend in (a)(i) applies to (b)(i) and (c)(i); legend in (a)(ii) applies to (b)(ii) and (c)(ii)



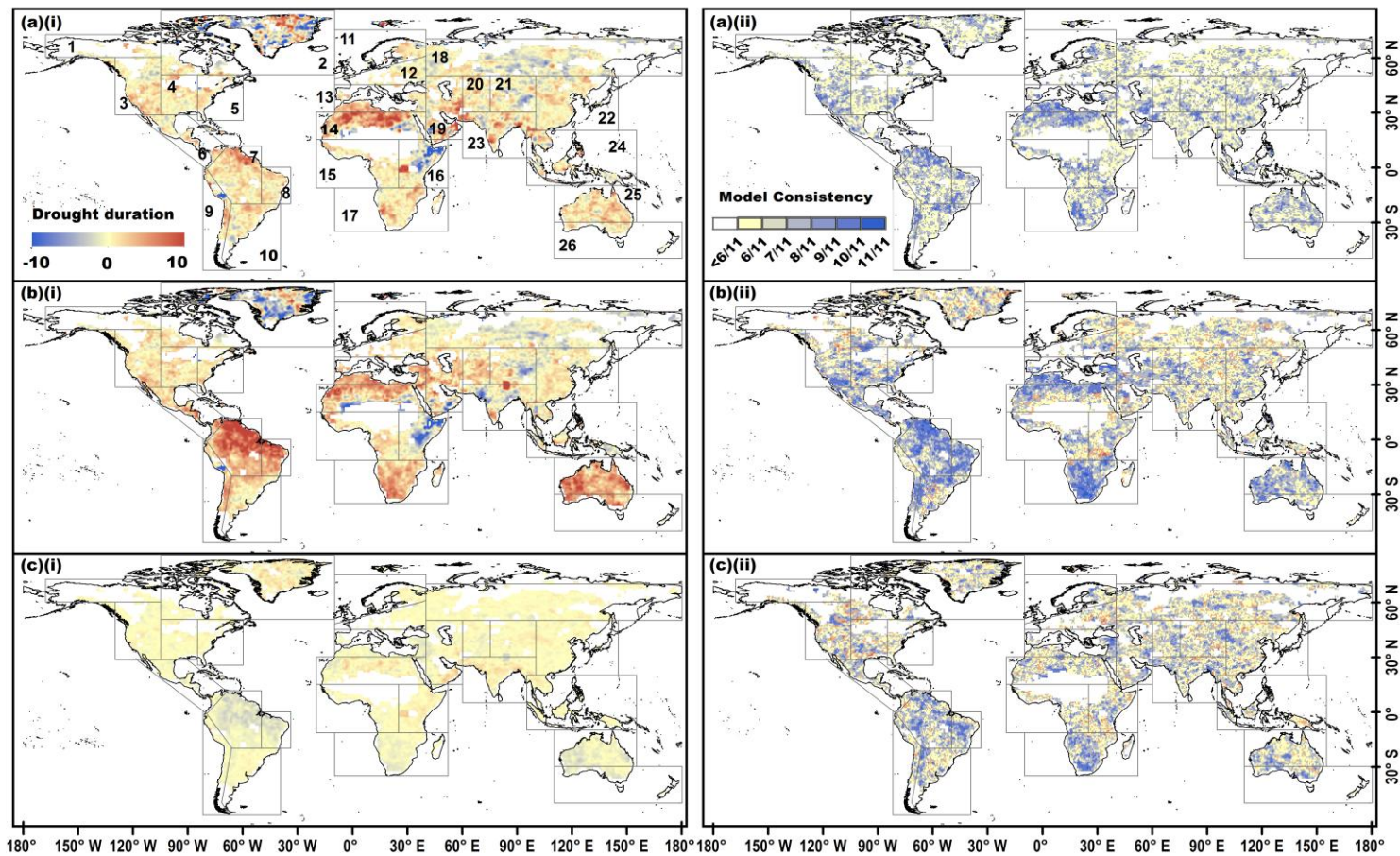
709
710

711 **Figure 4:** Multi-model projected PDSI at the globe (66°N-66°S) and in 27 world regions for the baseline period, 1.5°C and 2°C warmer worlds.
 712 The projected uncertainty of multiple climate models is shown through box plots for each region and for each period



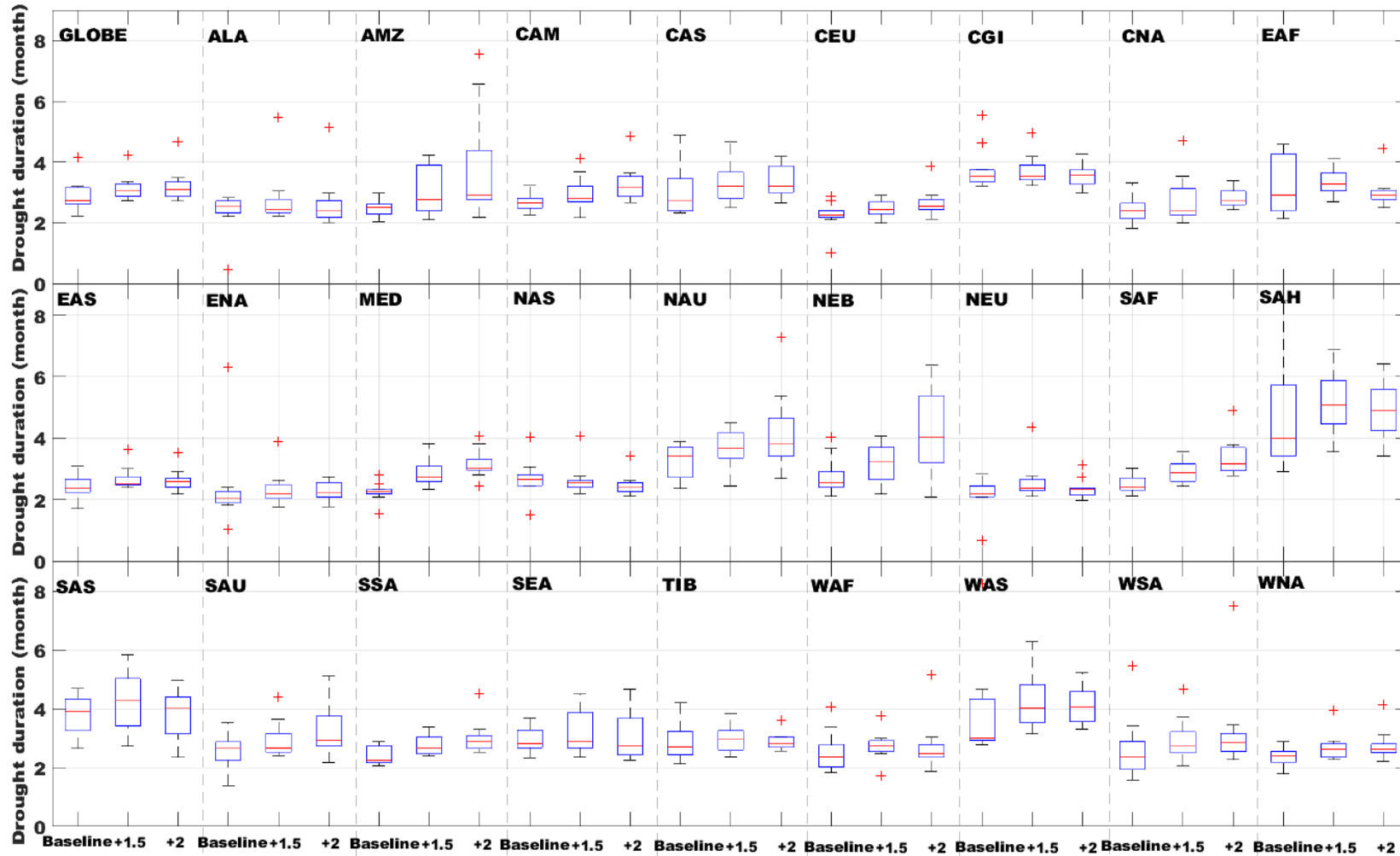
713

714 **Figure 5:** Changes in multi-model ensemble mean drought duration (months) (i) and model consistency (ii) on a spatial resolution of $0.5^\circ \times 0.5^\circ$,
 715 (a) from the baseline period to 1.5°C warmer world, (b) from the baseline period to 2°C warmer world and (c): (a)-(b). The dark-gray boxes
 716 show the regions adopted by IPCC (2012), which are labeled in (a)(i) using the ID numbers defined in Table 2. Legend in (a)(i) applies to (b)(i)
 717 and (c)(i); legend in (a)(ii) applies to (b)(ii) and (c)(ii)



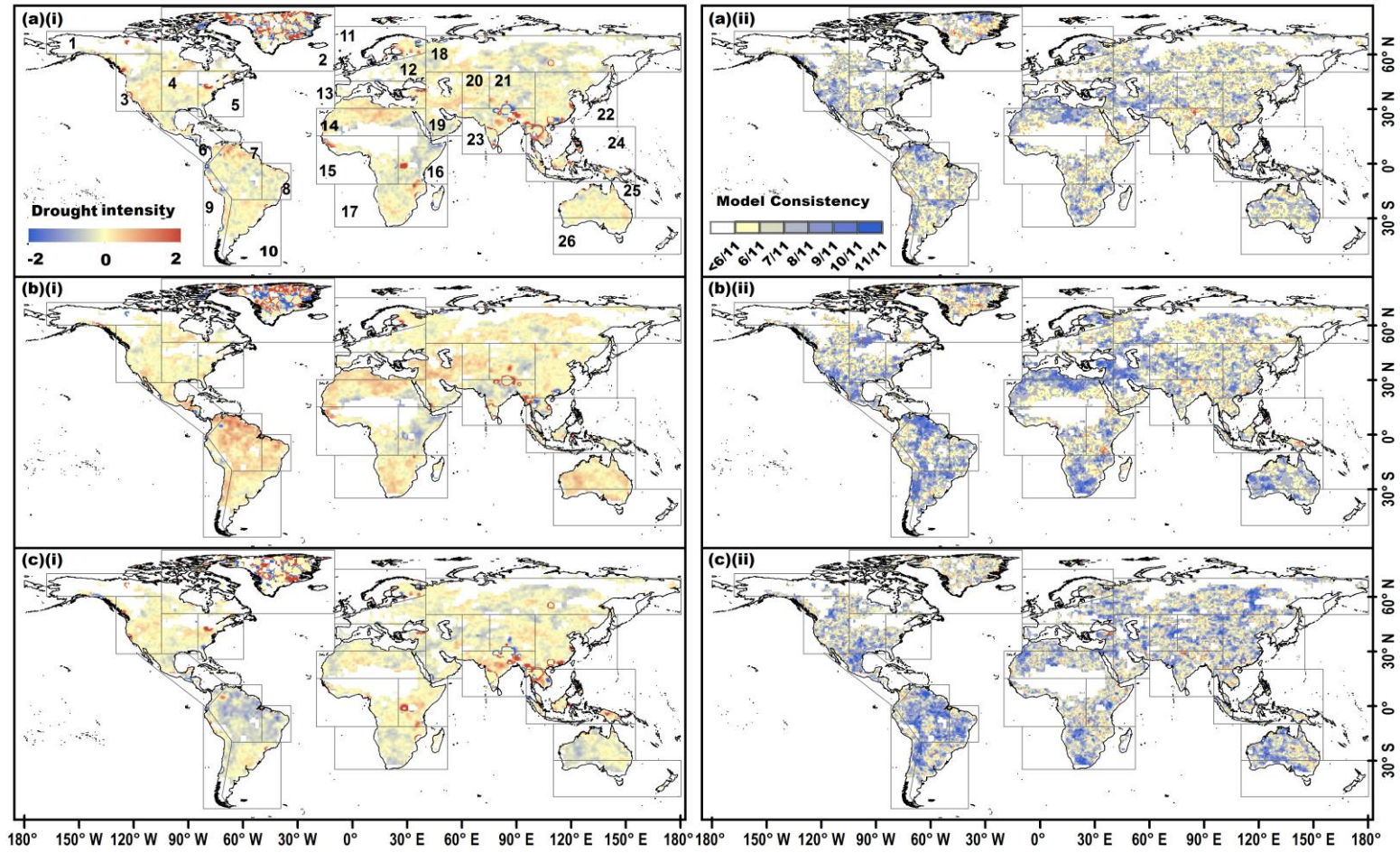
718
 719

720 **Figure 6:** Multi-model projected drought duration (months) at the globe (66°N-66°S) and in 27 regions for the baseline period, 1.5°C and 2°C
 721 warmer worlds. The projected uncertainty of multiple climate models is shown through box plots for each region and for each period



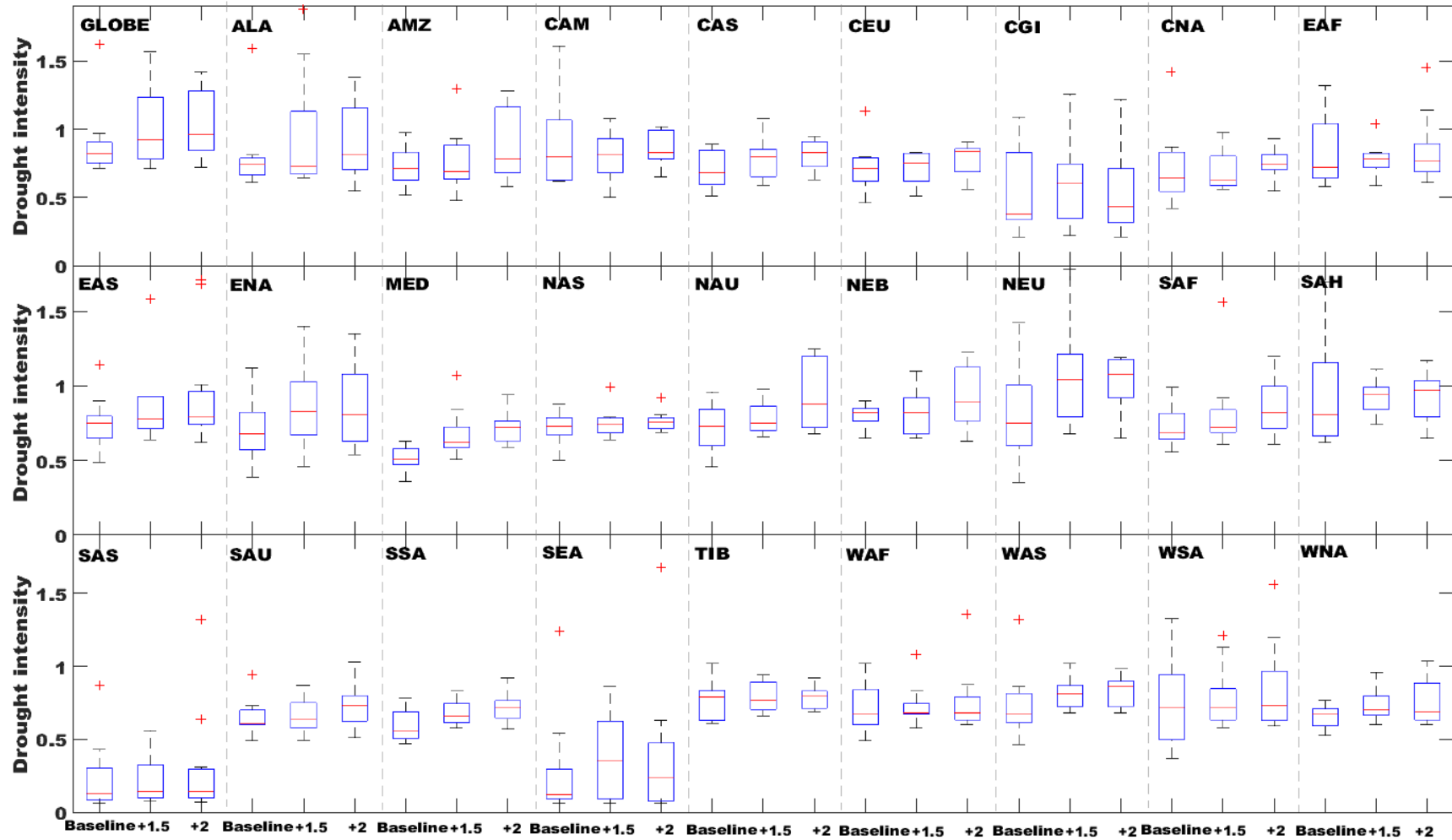
722

723 **Figure 7:** Changes in multi-model ensemble mean drought intensity (dimensionless) (i) and model consistency (ii) on a spatial resolution of 0.5°
 724 $\times 0.5^\circ$, (a) from the baseline period to 1.5°C warmer world, (b) from the baseline period to 2°C warmer world and (c): (a)-(b). The dark-gray
 725 boxes show the regions adopted by IPCC (2012), which are labeled in (a)(i) using the ID numbers defined in Table 2. Legend in (a)(i) applies to
 726 (b)(i) and (c)(i); legend in (a)(ii) applies to (b)(ii) and (c)(ii)



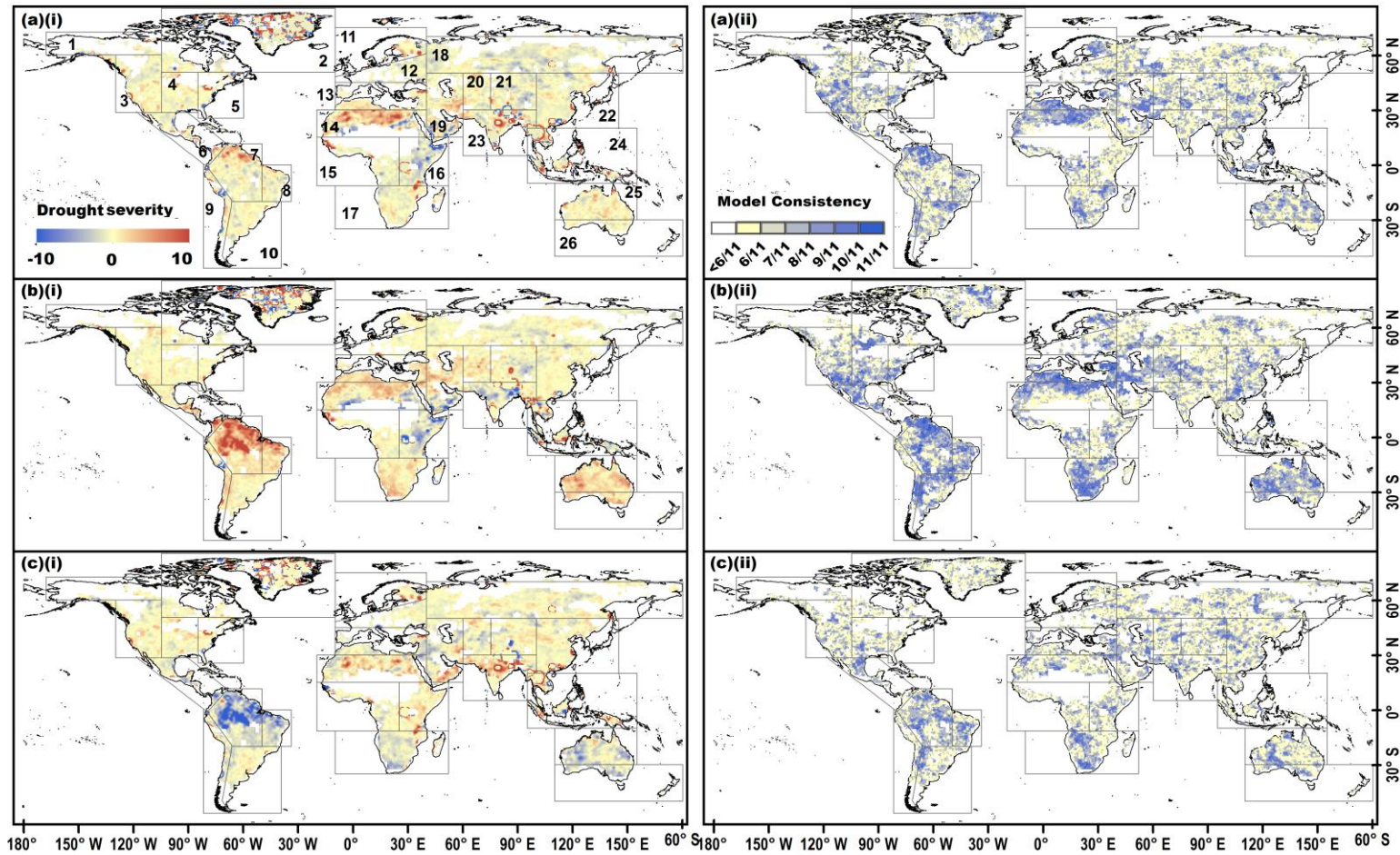
727

728 **Figure 8:** Multi-model projected drought intensity (dimensionless) at the globe (66°N-66°S) and in 27 regions for the baseline period, 1.5°C and
 729 2°C warmer worlds. The projected uncertainty of multiple climate models is shown through box plots for each region and for each period



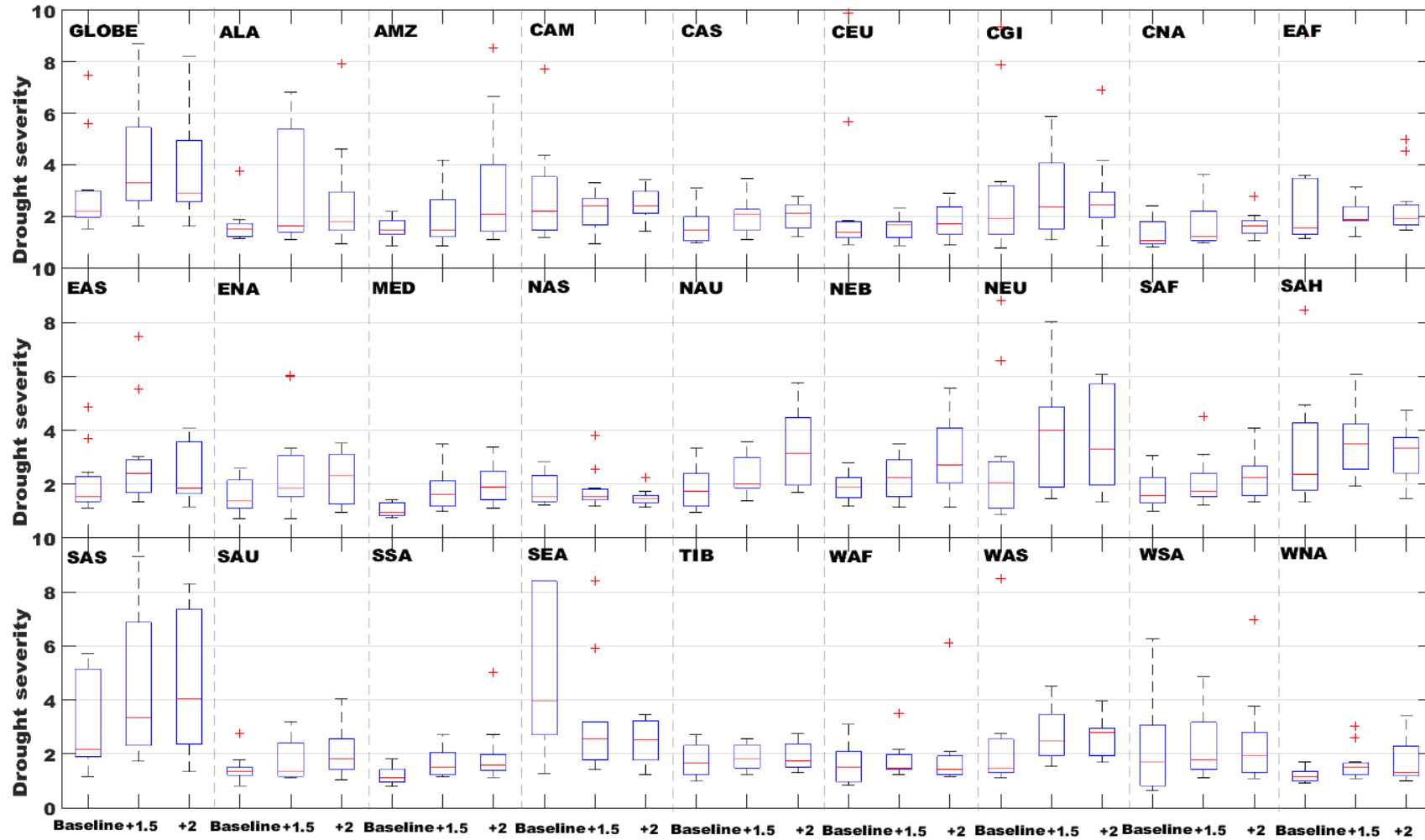
730

731 **Figure 9:** Changes in multi-model ensemble mean drought severity (dimensionless) (i) and model consistency (ii) on a spatial resolution of 0.5°
 732 $\times 0.5^\circ$, (a) from the baseline period to 1.5°C warmer world, (b) from the baseline period to 2°C warmer world and (c): (a)-(b). The dark-gray
 733 boxes show the regions adopted by IPCC (2012), which are labeled in (a)(i) using the ID numbers defined in Table 2. Legend in (a)(i) applies to
 734 (b)(i) and (c)(i); legend in (a)(ii) applies to (b)(ii) and (c)(ii)



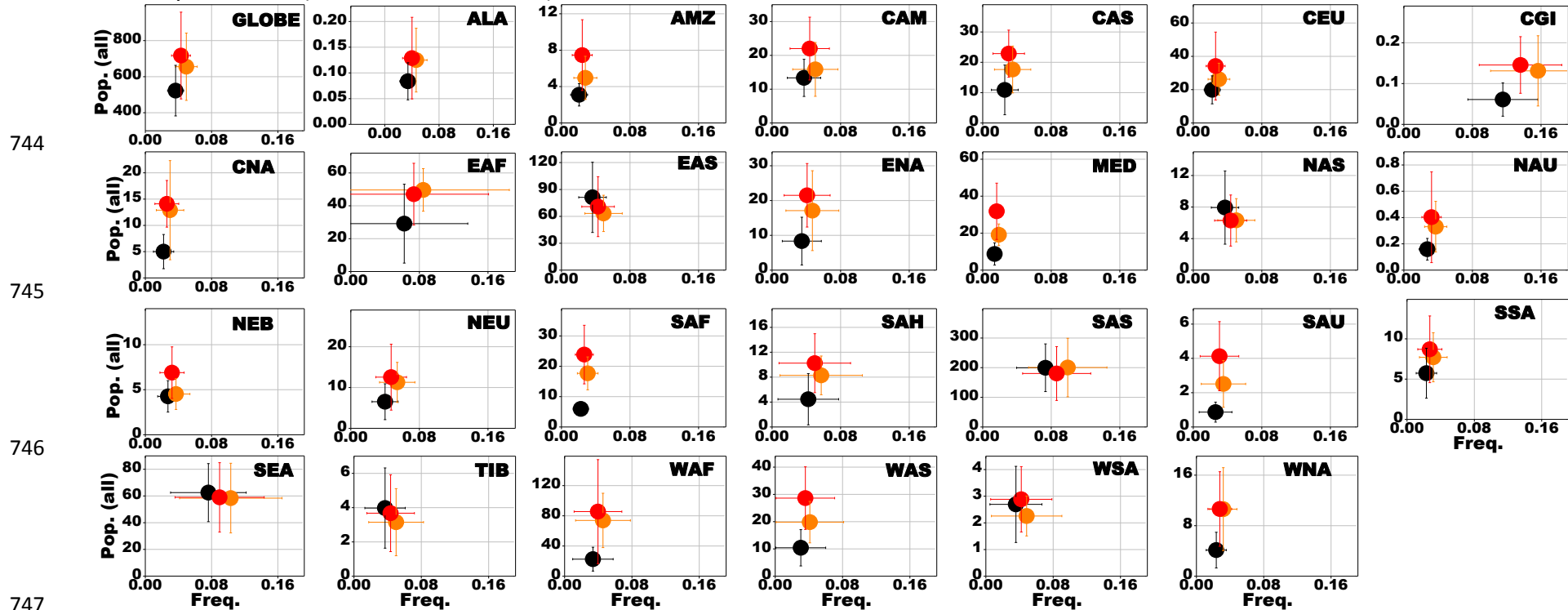
735

736 **Figure 10:** Multi-model projected drought severity (dimensionless) at the globe (66°N-66°S) and in 27 regions for the baseline period, 1.5°C and
 737 2°C warmer worlds. The projected uncertainty of multiple climate models is shown through box plots for each region and for each period

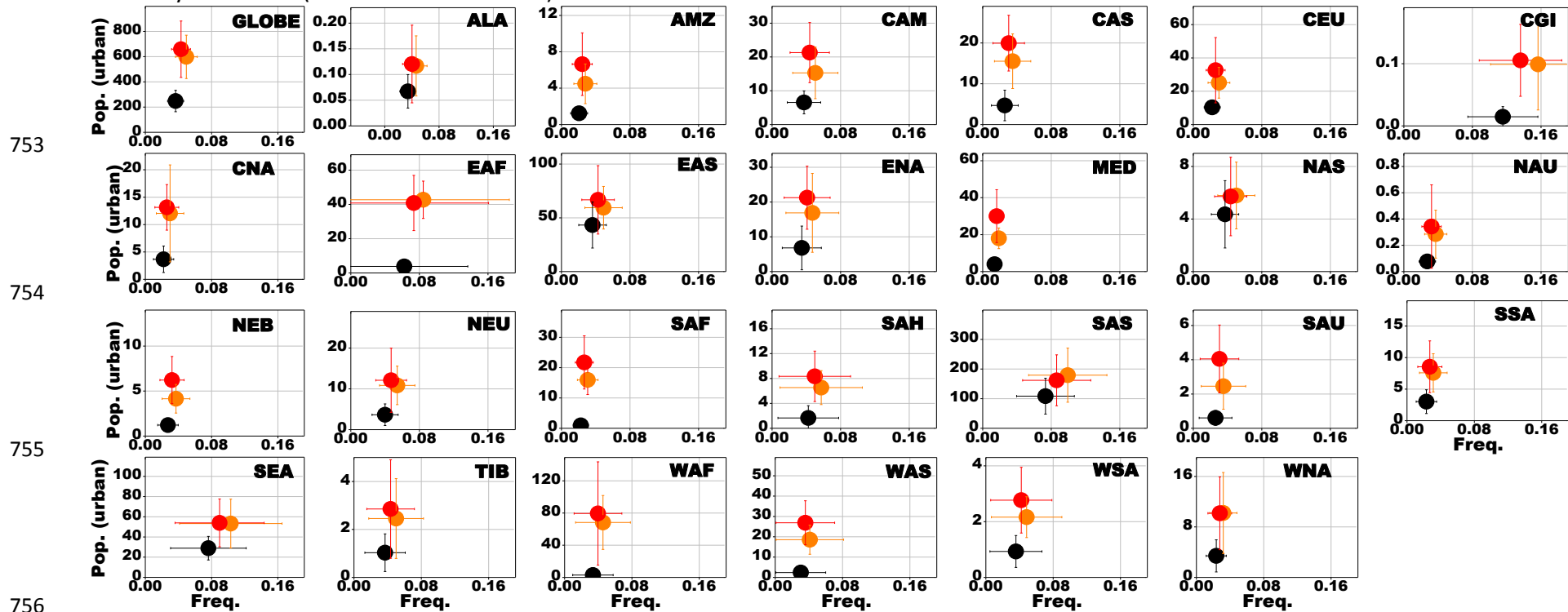


738
739

740 **Figure 11:** Multi-model projected frequency (Freq.) and affected total population (Pop., million) of severe drought (PDSI < -3) at the globe and in 27 regions for the baseline period (black, fixed SSP1 2000 population), 1.5°C (orange, fixed SSP1 2100 population) and 2°C (red, fixed SSP1 2100 population) warmer worlds. The projected uncertainties (standard deviation of multiple-model results) of multiple climate models are shown by error bars (horizontal and vertical)



749 **Figure 12:** Multi-model projected frequency (Freq.) and affected urban population (Pop., million) of severe drought (PDSI < -3) at the globe and
 750 in 27 regions for the baseline period (black, fixed SSP1 2000 population), 1.5°C (orange, fixed SSP1 2100 population) and 2°C (red, fixed SSP1
 751 2100 population) warmer worlds. The projected uncertainties (standard deviation of multiple-model results) of multiple climate models are
 752 shown by error bars (horizontal and vertical)



756
757

758 **Figure 13:** Multi-model projected frequency (Freq.) and affected rural population (Pop., million) of severe drought (PDSI < -3) at the globe and in 27 regions for the baseline period (black, fixed SSP1 2000 population), 1.5°C (orange, fixed SSP1 2100 population) and 2°C (red, fixed SSP1 2100 population) warmer worlds. The projected uncertainties (standard deviation of multiple-model results) of multiple climate models are shown by error bars (horizontal and vertical)

